



Tectonics

RESEARCH ARTICLE

10.1002/2016TC004236

Key Points:

- Reconstruction of the thermotectonic history along the Amundsen Sea Coast
- Time-temperature modeling suggests late Cretaceous postorogenic gravitational collapse
- Low-temperature thermochronology reveals Cenozoic crustal tilting in Pine Island Bay

Supporting Information:

- Supporting Information S1

Correspondence to:

J. Lindow,
lindow.julia@outlook.com

Citation:

Lindow, J., P. J. J. Kamp, S. B. Mukasa, M. Kleber, F. Lisker, K. Gohl, G. Kuhn, and C. Spiegel (2016), Exhumation history along the eastern Amundsen Sea coast, West Antarctica, revealed by low-temperature thermochronology, *Tectonics*, 35, 2239–2257, doi:10.1002/2016TC004236.

Received 12 MAY 2016

Accepted 30 AUG 2016

Accepted article online 31 AUG 2016

Published online 6 OCT 2016

Exhumation history along the eastern Amundsen Sea coast, West Antarctica, revealed by low-temperature thermochronology

Julia Lindow¹, Peter J. J. Kamp², Samuel B. Mukasa³, Michel Kleber¹, Frank Lisker¹, Karsten Gohl⁴, Gerhard Kuhn⁴, and Cornelia Spiegel¹

¹Department of Geosciences, University of Bremen, Bremen, Germany, ²School of Science, University of Waikato, Hamilton, New Zealand, ³College of Engineering and Physical Sciences, University of New Hampshire, Durham, New Hampshire, USA, ⁴Alfred Wegener Institute Helmholtz-Centre for Polar and Marine Research (AWI), Bremerhaven, Germany

Abstract West Antarctica experienced a complex tectonic history, which is still poorly documented, in part due to extensive ice cover. Here we reconstruct the Cretaceous to present thermotectonic history of Pine Island Bay area and its adjacent coasts, based on a combination of apatite and zircon fission track and apatite (U-Th-Sm)/He thermochronology. In addition, we report petrographic information for the catchments of Pine Island, Thurston Island, and Thwaites glaciers. Our data suggest that the underlying bedrock of the Pine Island and Thwaites Glacier catchments are very different and vary from granitoids to (Cenozoic?) volcanogenic sequences and low-grade metamorphics. Our thermochronology data show that the upper crustal rocks of Pine Island Bay experienced very rapid cooling during the late Cretaceous. We attribute this rapid cooling of basement rocks and associated reduction in mean elevation to tectonic denudation driven by gravitational collapse of the Cretaceous orogen along the proto-Pacific Gondwana margin. Rapid Cretaceous crustal cooling was followed by very slow cooling during the Cenozoic, with no erosional response—within the limits of thermochronological methods—to the onset of glaciation and subsequent climatic changes. Cenozoic rifting within the West Antarctic Rift appears to have had little effect on erosion processes around Pine Island Bay; instead, our data suggest Cenozoic crustal tilting toward Pine Island Trough, a major geomorphic feature previously suggested to be a branch of the rift system.

1. Introduction

The Amundsen Sea (Figure 1) of West Antarctica stretches over 1000 km along the present-day South Pacific rim. This area was influenced by all of the major tectonic events that formed present-day West Antarctica, including formation of a batholith belt resulting from magmatic processes associated with Paleozoic to Cretaceous subduction along the Gondwana margin [Mukasa and Dalziel, 2000; Dalziel and Lawver, 2001]. This area is also close to the zone of continental breakup of West Antarctica and New Zealand that followed the cessation of subduction, and it was also affected by Cretaceous to recent extension within the West Antarctic Rift System. Extension has resulted in thinned crust beneath the area, its low-lying topography, and deeply incised valleys [e.g., Winberry and Anandakrishnan, 2004; Jordan et al., 2010; Chaput et al., 2014, and references therein]. Many details of West Antarctica's geodynamic history remain hidden under 1–4 km of the West Antarctic Ice Sheet, such as the extent and amount of possible subduction-related uplift and erosion, and the location and timing of rifting. Also, even basic information about the distribution of lithologic units constituting West Antarctica is lacking and limited to ice-free outcrops (nunataks), coastal cliffs, and some islands, together forming less than 2% of the continental area.

The unique setting of rifted bedrock underlying ice by 0.5 to 1.5 km below sea level makes the West Antarctic Ice Sheet particularly sensitive to subglacial intrusion of warm ocean water along tectonic rift structures, thereby inducing bottom melting [LeMasurier, 2006, 2008; Bingham et al., 2012; Fretwell et al., 2013]. The Amundsen Sea coast is already characterized by ice sheets with rapid grounding line retreat and enhanced thinning [e.g., Rignot et al., 2011, 2013]. These characteristics and the fact that most of the West Antarctic Ice Sheet is grounded below sea level combined with landward dipping coastal bedrock set up the potential for positive feedbacks. When relatively warm ocean water reaches the grounded base of ice sheets (grounding zone), the bottom melt leads to a destabilization of the grounding zone and thereby drives it further inland. The landward retreat of grounded ice further reduces the buttressing effect it has for the whole ice

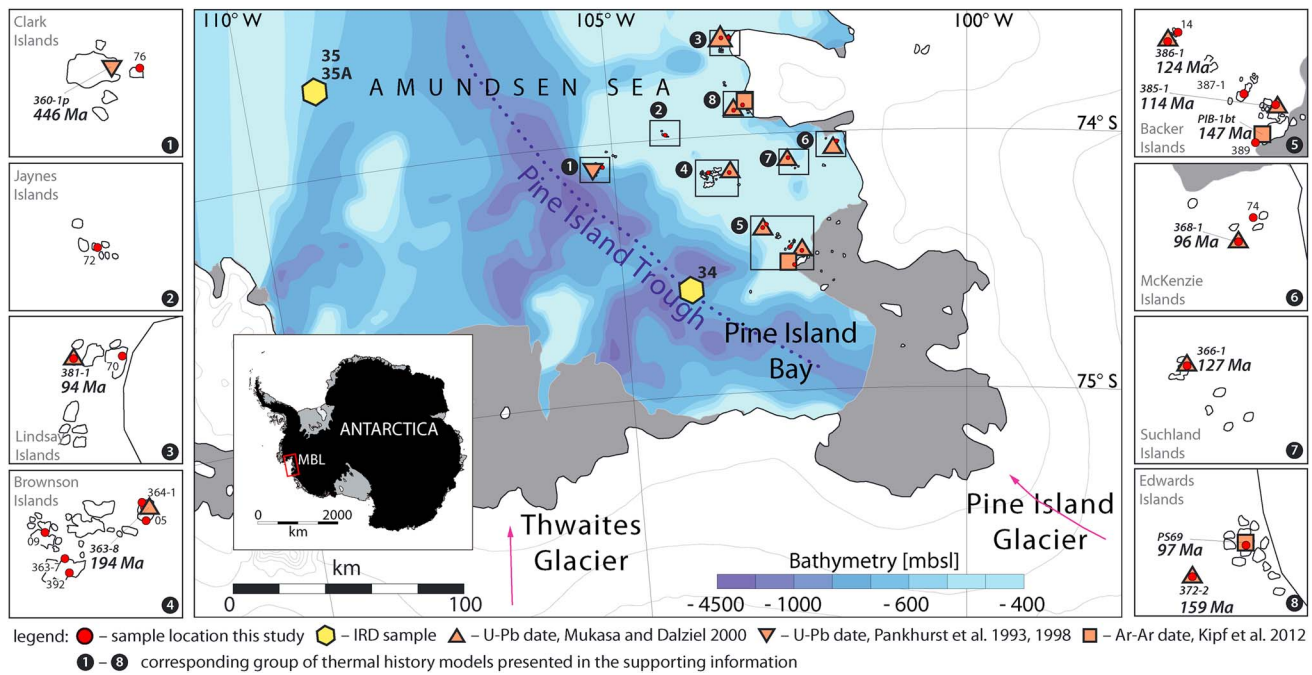


Figure 1. Overview map of the Pine Island Bay area, eastern Marie Byrd Land, West Antarctica. Contours are shown in gray with 250 m spacing. Pink arrows indicate flow directions of glaciers; ice shelves are shaded in gray. The modern grounding line (black continuous line) and regional bathymetry data are from *Rignot et al.* [2011] and *Nitsche et al.* [2007]. Bathymetry grading is adopted from *Smith et al.* [2011]. Blue dotted line follows the Pine Island glacial trough. Inset highlights study area on the Antarctic continent; MBL—Marie Byrd Land. Red dots mark the location of samples dated in this study, and orange symbols show sample locations of earlier studies [*Pankhurst et al.*, 1993, 1998; *Mukasa and Dalziel*, 2000; *Kipf et al.*, 2012] (see legend). Yellow hexagons are the locations of box cores of ice rafted debris (IRD). Boxes highlight individual areas shown in more detail in the maps on the left and right margin. The solid circle numbers refer to groups of thermal history models presented in the supporting information (Figure S5). Detailed maps bear location names, sample symbols, and sample names. Additionally, age data from earlier studies are shown in bold italic.

sheet, and it could induce a partial or full collapse of the West Antarctic Ice Sheet, leading to sea level rise of up to ~3.3 m [*Weertman*, 1974; *Mercer*, 1978; *Hughes*, 1981; *Bamber et al.*, 2009; *Joughin and Alley*, 2011]. For these reasons, the seafloor morphology and structure of Pine Island Bay (Amundsen Sea area) is of increasing interest, particularly as it includes vulnerable glacial systems (e.g., Pine Island and Thwaites Glaciers) [e.g., *Warner and Roberts*, 2013; *Favier et al.*, 2014; *Mouginot et al.*, 2014].

Striking roughly NW-SE, Pine Island Bay covers an area of approximately 20,000 km² and marks the calving grounds of Pine Island Glacier (Figure 1). The glacial valley beneath the main trunk of Pine Island Glacier originates from crustal extension [*Jordan et al.*, 2010] enhanced by subglacial erosion. This valley extends into Pine Island Bay and forms Pine Island Trough (Figure 1). Both structures, the valley beneath the main trunk of the glacier and Pine Island Trough, are considered to be a former and possibly still active rift arm of the much larger West Antarctic Rift System [e.g., *Jordan et al.*, 2010; *Gohl*, 2012] (Figures 1 and 2). Recent studies report crustal thicknesses for Pine Island Bay area of about 19–26 km [*Jordan et al.*, 2010] and 20–24 km [*Chaput et al.*, 2014]. Several groups of low-relief islands occur in Pine Island Bay, the majority of which are aligned along Pine Island Trough or are located perpendicular to it. Generally, the islands rise no more than 50 m above sea level; the few exceptions reach elevations above 100 m above sea level. The dominant bedrock lithology of these islands is coarse-grained granite of Mesozoic, mostly Cretaceous, age [*Mukasa and Dalziel*, 2000].

The absence of stratigraphic marker horizons limits the means for reconstructing the kinematic evolution of Pine Island Bay, making a thermochronology approach particularly suitable for deciphering the exhumation and denudation history of the field area. Low-temperature thermochronology provides a means to track the passage of rocks through the thermal structure of the upper crust, with which it interacts, and can in some circumstances help constraint lower crustal movements. In this paper we have applied three methods: apatite (U-Th-Sm)/He, and apatite and zircon fission track analysis in combination to concentrates from the same samples, which has enabled us to investigate cooling and exhumation histories in detail. The number and distribution of island groups in Pine Island Bay (Figure 1) provide a useful opportunity to investigate

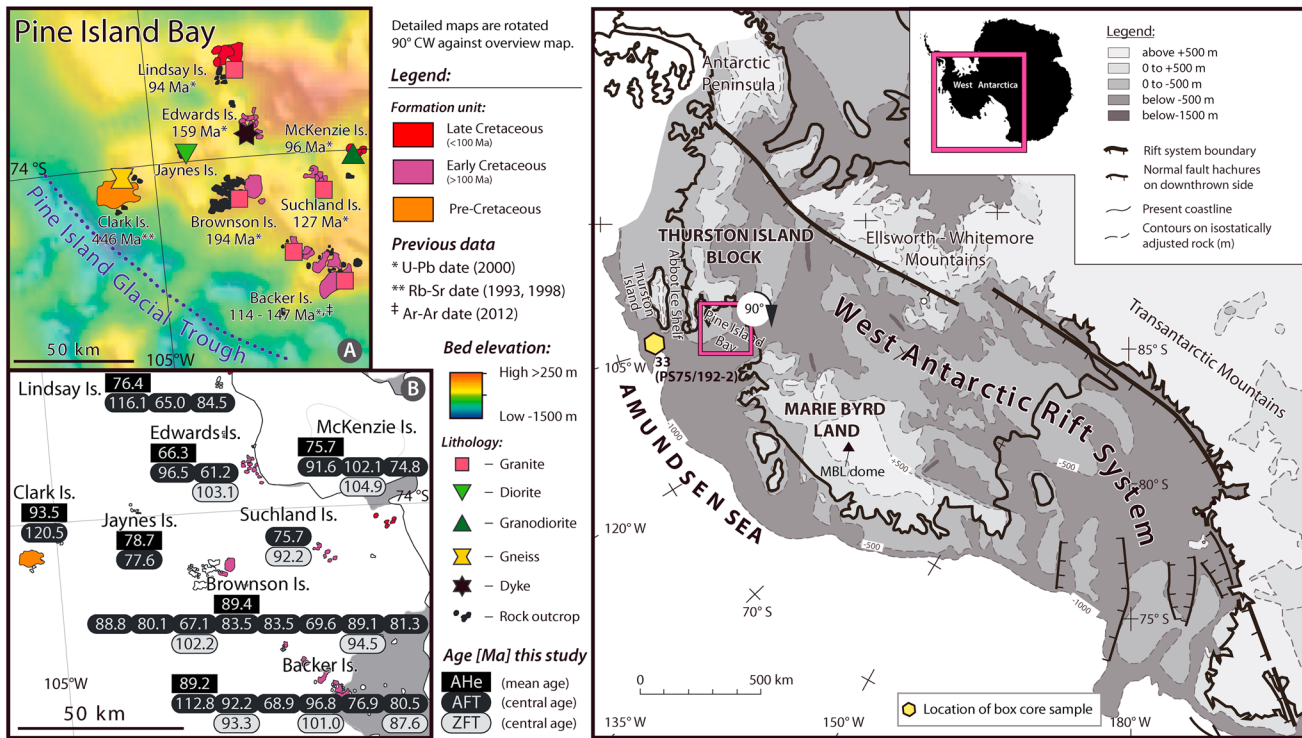


Figure 2. (right) Tectonic overview map of West Antarctica from *LeMasurier* [2008]; ice-free bed elevation is isostatically adjusted. Red rectangle marks the study area, also shown in more detail on the left side. (left) Detailed maps. (A) shows BEDMAP2 [Fretwell et al., 2013] bed elevation, major rock outcrops, sampled lithology, and corresponding formation with sample sites and results of earlier studies [Pankhurst et al., 1993, 1998; Mukasa and Dalziel, 2000; Kipf et al., 2012] (see legend) in Pine Island Bay. Blue dotted line follows the Pine Island Glacial Trough. (B) Geologic map of Pine Island Bay with location names, corresponding formation and results of thermochronological analysis. Black boxes: apatite (U-Th-Sm)/He ages, black rounded boxes: apatite fission track ages; and gray rounded box: zircon fission track ages. Note: detailed maps have been rotated 90° CW against the overview map.

local tectonics along orthogonal profiles to identify faults and to infer their impact on the present-day geomorphology of the area. To complement this data set, we have sampled ice-transported debris from the marine part of the bay to gain insights into the timing and magnitude of vertical crustal movement and erosion of basement beneath ice-covered catchment areas of Pine Island and Thwaites glaciers.

In this paper we present the first comprehensive thermochronologic data set about Pine Island Bay and its adjoining coasts deriving the Cretaceous-Cenozoic geodynamic history. Based on time-temperature paths modeled from our thermochronology data, we infer Cenozoic rift-related block faulting in Pine Island Bay, which supports the hypothesis that Pine Island trough is a branch of the West Antarctic Rift System. Finally, through thermal history inversions we estimate Cenozoic cooling rates of the basement and comment upon the erosional response to West Antarctic glaciation.

2. Setting and Background

2.1. Geologic and Tectonic History

Dalziel and Elliot [1982] identified four distinct crustal blocks in West Antarctica: Antarctic Peninsula, Ellsworth-Whitmore Mountains, Thurston Island, and Marie Byrd Land (Figure 2). The crustal boundary between Marie Byrd Land and the Thurston Island Block is assumed to be along Pine Island Bay [Grunow et al., 1991]. Prior to Gondwana breakup (180 Ma) [Lawver et al., 1991], the four blocks of West Antarctica formed the southeastern part of the active margin of Gondwanaland. Since at least the Devonian, Phoenix plate (proto-Pacific) lithosphere was subducted beneath Gondwana, resulting in large diorite, granodiorite, and monzogranite magmatic bodies, which today form most of the upper crustal outcrops of West Antarctica [Mukasa and Dalziel, 2000; Dalziel and Lawver, 2001]. The Cretaceous change from compression to extension induced and finally led to the separation of West Antarctica from New Zealand within only about 20 Myr between 101 ± 1 Ma and 81 ± 1 Ma [Mukasa and Dalziel, 2000, and reference therein]. According to

Eagles *et al.* [2004] and Wobbe *et al.* [2012], the first oceanic crust between Zealandia (i.e., the New Zealand continental block, including Campbell Plateau, Chatham Rise, North Island, and South Island; see supporting information for overview map of locations, Figure S1) and West Antarctica was formed at about 90–87 Ma in eastern Amundsen Sea between Chatham Rise and the Amundsen Sea Embayment and at 84 Ma between Campbell Plateau and Marie Byrd Land (Figure S1). Breakup was associated with further magmatic activity expressed on land as mafic dykes, which cut granitoids throughout Marie Byrd Land [Kalberg and Gohl, 2014].

Prior to and after continental breakup, an erosional surface developed on both the New Zealand and West Antarctic sides, beveling mid-Cretaceous and older basement rocks and forming the characteristic flat summits of present-day Marie Byrd Land. The West Antarctic Erosion Surface [LeMasurier and Landis, 1996] is preserved along a 2.5 km belt of the Amundsen Sea area with near coastal elevations between 400 and 1000 m. Based on sediment records from the New Zealand margin, the erosional surface formed at low elevations close to sea level between 85 Ma and the earliest Miocene, representing a period of tectonic stability and erosional leveling at a time before and subsequent to the separation of New Zealand from West Antarctica [LeMasurier and Landis, 1996; Landis *et al.*, 2008]. LeMasurier and Landis [1996] inferred a maximum regional uplift of approximately 3 km between the time of its formation and today.

Since the mid-Cretaceous, i.e., contemporaneous with the continental breakup described above and following it, the West Antarctic Rift System formed, displacing West Antarctica from East Antarctica. Published estimates for total crustal extension associated with the West Antarctic Rift System differ strongly and range between 120 and 1800 km [Storti *et al.*, 2008, and references therein]. Also, the total number and extent of rift valleys associated with this extensional deformation remains unknown, but the boundary between Marie Byrd Land and the Thurston Island Block, located in the Pine Island Bay area, was suggested as forming one of the branches that connects the interior of the West Antarctic rift system with the Amundsen Sea. However, detailed timing of this extensional activity remains largely unknown [Dalziel, 2006; Müller *et al.*, 2007; Jordan *et al.*, 2010; Gohl, 2012; Gohl *et al.*, 2013a, 2013b].

Most of crustal extension in the Pine Island Bay area was accompanied by mafic dyke formation. Cenozoic volcanic activity related to rifting started in Oligocene times and persists to present day. During the Oligocene, the southern rift shoulder of the rift system (i.e., the Transantarctic Mountains) was exhumed [Prenzel *et al.*, 2013, 2014]. In the Transantarctic Mountains (Figure S1), pre-Cenozoic basement reaches altitudes above 4 km before abruptly descending along its northern front to the rift floor some 0.5 to 1.5 km below sea level [LeMasurier, 1990]. North of Transantarctic Mountains, the highly elevated Marie Byrd Land dome (Figure 2; peak: 2.7 km) has been considered to mark the northern rift shoulder [LeMasurier, 2006], but nowadays it is viewed as an intrarift dome comparable to Kenyan and Ethiopian domes [LeMasurier, 2008]. Dome uplift has been suggested to have commenced during the mid-Oligocene (28–30 Ma) [LeMasurier and Landis, 1996], coeval with block faulting and the onset of basaltic volcanism in the area [LeMasurier and Landis, 1996]. Today, West Antarctica is characterized by active volcanism and a crustal thickness that varies between 21 and 28 km (measured across central Marie Byrd Land normal to the Transantarctic Mountain front) [Chaput *et al.*, 2014].

2.2. Continental Glaciation

Large continental ice caps in Antarctica are considered to have first formed during the early Oligocene [Zachos *et al.*, 2001; Wilson *et al.*, 2013]. They persisted until the mid-Oligocene before global warming reduced them in both volume and areal extent until 15 Ma. After the Miocene climatic optimum (17–15 Ma) [Zachos *et al.*, 2001], global climate gradually cooled, which led to establishment of extended ice sheets on Antarctica. Small-scale changes in extent of the West Antarctic Ice Sheet were induced by cooling at the Miocene-Pliocene boundary [Zachos *et al.*, 2001]. Today, the glaciers draining into the Amundsen Sea are characterized by the highest mass losses of all glaciers draining the Antarctic continent and are associated with rapid thinning and grounding line retreat [e.g., Rignot *et al.*, 2008; Pritchard *et al.*, 2009; Joughin *et al.*, 2010; Favier *et al.*, 2014].

3. Methods

3.1. Low-Temperature Thermochronology

We applied low-temperature thermochronology, using three systems in combination: zircon fission track (ZFT), apatite fission track (AFT), and apatite (U-Th-Sm)/He dating (AHe), for thermal history reconstruction,

which helps to derive a geodynamic evolution of West Antarctica. All three techniques are based on temperature-dependent accumulation of radioactive decay products over time, providing information on how much time has passed since a sample host rock was at a specific ambient temperature in the upper crust, and therefore, assuming a geothermal gradient, at a certain crustal depth. The three methods are sensitive to different temperature intervals, with ZFT thermochronology being sensitive to temperatures between 330 and 230°C [Tagami and Shimada, 1996], AFT between 120 and 60°C [e.g., Wagner et al., 1989], and AHe thermochronology to temperatures between ~85 and 40°C [e.g., Wolf et al., 1998; Farley, 2002]. Because temperature sensitivities of the AFT and AHe systems overlap, thermal histories based on a combination of these two methods are particularly well constrained. Together with ZFT thermochronology, the three methods provide compelling information that allows us to deduce geodynamic movements within the upper ~1.5 to 11 km of the crust, assuming a geothermal gradient of 30°C/km. Some of the samples analyzed in this study were previously dated by zircon U/Pb geochronology, providing additional constraints on the thermal history at temperatures around 900°C [Mukasa and Dalziel, 2000]. For AFT thermochronology, mean lengths of fission tracks and their shortening patterns give additional information on the thermal history experienced by the sample [Laslett et al., 1982; Gleadow et al., 1986]. As a measure of annealing properties of fission tracks in apatite, we used the etching velocities expressed as etch pit diameter parallel to the crystallographic *c* axis (D_{par} value) [Burtner et al., 1994; Donelick et al., 2005]. Methodological details and laboratory procedures used in this investigation are summarized in supporting information Texts S1 and S2, including also a more detailed discussion [Taylor, 1969; Wagner et al., 1989; Hurford, 1990; Cherniak, 1993; Brabander and Giletti, 1995; Farley et al., 1996; Eggins et al., 1997; Lovera et al., 1997; Shuster et al., 2006; Ketcham et al., 2007b; Vermeesch, 2008].

3.2. Thermal History Modeling

The different thermochronological dating systems applied here can be integrated by thermal history modeling using algorithms that describe track annealing and helium diffusion in the dated mineral. For this study we used the annealing algorithms of Ketcham et al. [2007a], the stopping distances from Ketcham et al. [2011], and the diffusion model of Flowers et al. [2009] to account for potential effects of radiation damage on diffusion characteristics. By using HeFTy version 1.8.3 (program by Ketcham [2005]), we applied inverse thermal history modeling for all individual samples with AHe, AFT, and/or ZFT data, including track length measurements and information on the kinetic parameter (D_{par}).

Additional constraints provided by published Ar-Ar, Rb-Sr, and zircon U/Pb data from Pine Island Bay (1993) [Pankhurst et al., 1998; Mukasa and Dalziel, 2000; Kipf et al., 2012] (see supporting information for details) have also been used in thermal history modeling. Potential solutions are differentiated into “acceptable” and “good” paths according to their goodness-of-fit between the model and measured parameters. A “good” result can be interpreted as a time-temperature path supported by the measured data, while an acceptable path is not ruled out by the input data [Ketcham, 2005]. A compilation of all modeling results is shown in Figure S5 in the supporting information.

3.3. Detrital Clast Analysis

A moving ice mass, such as a glacier, incorporates clasts of different types and various sizes into its sediment load, which are released and deposited in the marine realm as part of the ice calving process. This so called “ice rafted debris” (IRD) derives from different locations across the hinterland glacial catchment and carries information about source area’s geology and exhumation history, which are otherwise inaccessible due to the ice cover. After debris has been deposited on shelf areas or in deeper water environments, it becomes accessible by coring.

For this study, IRD was obtained from box corers and sieved into fractions of >20 mm, 10–20 mm, 5–10 mm, and 2–5 mm. The various fractions were then thoroughly washed and dried, the clasts then being sieved to remove residual marine mud. This was followed by weighting and modal analysis ($n \sim 1000$ for each sample) to determine petrographic composition for each sample. AFT dating was undertaken on each sample to identify the main cooling age populations. In statistical analysis and visualization of the fission track detrital age distributions, binomial peak fitting [Brandon, 1996] was applied to the single-grain age data. The *F* test was used to determine the optimal number of age groups present in a sample [Brandon, 1992, 2002].

4. Sampling

Although exploration of Marie Byrd Land commenced in 1902, the Amundsen Sea area is still one of the least visited regions in Antarctica. RV *Polarstern* cruise ANT-XXVI/3 in 2010 provided a rare opportunity for onshore geological fieldwork in the Amundsen Sea area, 20 years after the SPRITE campaign [SPRITE-Group and Boyer, 1992]. We sampled mainly coarse-grained granites, often containing mafic xenoliths, which form the most common lithology in Pine Island Bay. These rocks belong to the I-type granitoid intrusions of the West Antarctic batholith belt and show zircon U-Pb lower intercept ages of middle to late Mesozoic [Mukasa and Dalziel, 2000]. The only exception to this pattern is a strongly deformed gneiss sampled from Clark Island close to the Pine Island Trough (Figure 1), which has a Rb-Sr age of 446 Ma [Pankhurst et al., 1998]. Our sampling strategy should enable us to detect crustal tilting or displacement of basement if existent, because in Pine Island Bay we sampled from low elevations only and along two orthogonal profiles. For thermochronology analysis of basement, we took samples of up to 10 kg to ensure that a sufficient amount of apatite and zircon would be obtained.

The samples from cruise ANT-XXVI/3 (MBL, short for Marie Byrd Land, sample codes) were complemented by samples collected during the SPRITE expedition to Pine Island Bay in 1992 (MB, short for Marie Byrd Land, sample codes). Together, this study comprises 34 bedrock samples from 12 different islands. Furthermore, we analyzed ice rafted debris (IRD) from three box corers deployed in depths between 450 and 800 m below sea level during the ANT-XXVI/3 expedition in Pine Island Bay (Figures 1 and 2 and Table S2). One IRD sample was taken next to Pine Island glacial trough and directly in front of the Pine Island Glacier outlet (Figure 1). The second sample received detritus from the catchment of Thwaites Glacier (Figure 1). It originates from an area that used to be covered by the Thwaites Iceberg Tongue and was recently ice free for the first time in at least 55 years. The upper 10 centimeters of the box core sampled near the Thwaites glacial trough were composed of brown sediments, in contrast to gray clay in the lower part. We interpret this color change as indicating the change from subglacial deposition beneath Thwaites Iceberg Tongue to deposition during at least partly ice-free conditions. To identify potential changes in transport pathways or source areas during deglaciation, we subsampled the upper part (MBL-35A-10) separately from the rest of the box core (MBL-35-10). A third box core was taken west of Thurston Island (Figure 2), drained from the Abbot Ice Shelf between Thurston Island and the adjacent peninsula. This sample reflects age patterns in the northern Thurston Island continental block, outside of Pine Island Bay in a strict sense. For the IRD compositional analysis we separated all clasts within box core samples between >20 mm, 10–20 mm, 5–10 mm, and 2–5 mm by sieving.

5. Petrography of Ice-Transported Clasts—Results and Interpretation

Some 4000 pebbles with a total mass of 26 kg were examined and classified. In varying amounts, all samples contain granitoid rocks, volcanogenic rocks, metamorphic rocks, and sedimentary rocks. The latter only occur in small amounts (3 to <1%) and are siliciclastic in composition. They are only weakly lithified and may represent reworked glaciomarine deposits. The next section provides an overview of sample composition including the corresponding coring site on cruise ANT-XXVI/3 (in square brackets). Detailed petrographic composition is presented in supporting information Table S2 and Figure S3.

5.1. MBL-33-10 [PS75/192-2], Derived From Thurston Island/Abbot Ice Shelf

The most frequently occurring clasts in this sample are of granitoid composition. Volcanogenic rocks are also abundant, mostly being of basaltic composition, buttrachytes, and rhyolites, as well as hyaloclastites also occur. For metamorphic rocks, low-grade metasediments such as quartzites are most common, and in addition, some large greenschist clasts (partly >20 mm) occur. The latter are mostly composed of chlorite and strongly altered amphibole. Generally, the clasts from this box core are mostly angular and relatively large compared with those from the other two box cores, possibly indicating a shorter transport distance.

The granitoid clasts from the box core largely match the lithological composition of outcrops on Thurston Island. However, no exposures of volcanic rocks have been described for Thurston Island [e.g., Lopatin and Orlenko, 1972], so they are most likely derived from Cenozoic volcanic complexes near Pine Island Glacier. No low-grade metamorphic rocks are exposed in the sediment source area, but they presumably comprised the host rocks for the Paleozoic to Mesozoic intrusive bodies.

5.2. MBL-34-10 [PS75/215-1], Derived From the Catchment of the Pine Island Glacier

MBL-34-10 is dominated by coarse-grained granite (~95%; Figure S3). The larger clasts are highly weathered and covered with a brownish crust, and some of them have remnants of organic growth long since expired. Volcanic and pyroclastic debris occur only in the 2–5 mm and 5–10 mm fractions and make up only ~1% by volume. The volcanic clasts are of rhyolitic/dacitic composition. Metamorphic rocks comprise small amounts of quartzite, orthogneiss, and greenschists. Compared with MBL-35(A)-10, the MBL-34-10 clasts are more rounded and altered. The pebbles in MBL-34-10 do not show much grain size variation.

Although Pine Island Glacier drains a very large catchment area ($20 \times 10^3 \text{ km}^2$) there are no basement exposures within it and hence IRD provide the only insights into subglacial lithologies. Because of Pine Island Glacier's, close vicinity to active volcanoes, we speculate that Pine Island Glacier sits on volcanic and/or sedimentary rocks. Without providing evidence against such lithologies, our data, however, strongly indicate a composition of the catchment area dominated by very similar granitoid rocks as exposed in Pine Island Bay, thus likely forming part of the batholith belt associated with the former Devonian to Cretaceous Gondwana margin.

5.3. MBL-35(A)-10 [PS75/219-2], Derived From the Catchment of the Thwaites Glacier

Sample MBL-35(A)-10 was subdivided into two samples at 10 cm depth in the box core. Petrographic analysis yielded practically identical pebble compositions for both subsamples with nearly equal amounts of igneous and metamorphic rocks (50% versus 45%; Figure S3). The majority of the igneous rocks (~23%) comprised pale-pink granites, white to grey granodiorites, and quartz-rich granites. Alkali-feldspar granite tonalite, quartz monzonite, and pegmatite form minor components. In comparison with MBL-34-10, the intrusives are richer in quartz. Some subvolcanic rocks occur in MBL-35-10. These are mainly composed of feldspar and pyroxene and are classified as dolerite. The volcanic rocks occur in nearly equal proportions—half andesitic/basaltic and half rhyolitic/dacitic. Pyroclast clasts are common (16%), being more abundant than volcanic rocks (11%) in this sample.

Metamorphic rocks dominate the second portion of sample MBL-35-10, and they are mainly metasediments such as metapelite, often containing secondary quartz veins. On some metasediment surfaces, remains of coral growth occur. Pyrite and chalcopyrite occur on several metapelite pebbles, suggesting an earlier history of hydrothermal activity. Several of the larger metapelite clasts show glacial striations of up to one centimeter in width. Other metasediments occurring in this sample are quartzites (2–3%) and phyllites (<1%). Furthermore, minor amounts of orthogneisses and greenschists are present. In the >10 mm fraction, a single chert pebble was found, and a clast with a reddish color seems to be entirely composed of filled vesicles with the former host rock being completely absent. However, the mineralogy of the fillings could not be identified. In general, the clasts are rounded and bear almost no signs of weathering.

The catchment area for Thwaites Glacier is as large as that for Pine Island Glacier (Figure 1) but contains at least two bedrock exposures, namely, Mount Takahe and Cray Mountains, providing the only direct information on bedrock geology. Both Mount Takahe and Cray Mountains are Cenozoic alkaline volcanic complexes, mainly comprising phonolytic to trachytic rocks, pyroclastic rocks and hyaloclastite [Palais *et al.*, 1988; Panter *et al.*, 2000]. However, volcanogenic rocks make up <30% of the pebbles from the box core. Instead, the clast compositions suggest that Cenozoic volcanic rocks were emplaced on top of granitoid rocks, again most likely belonging to the Paleozoic to Mesozoic batholith belt related to the Gondwana active margin. The batholiths, in turn, were most likely intruded into (Paleozoic?) low-grade metamorphic rocks, probably similar to those described from the Ross Sea area of Marie Byrd Land [Siddoway, 2008]. High-grade metamorphic rocks, as also described from the Ross Sea area, however, do not occur in the box core samples from Pine Island Bay.

6. Low-Temperature Thermochronology Results

6.1. Overview

We obtained a total of 43 low-temperature thermochronology ages for samples from the Pine Island Bay region (Figure 2 and Table S1). These comprise eight ZFT dates (Table 1) and 25 plus three AFT dates (Tables 2 and 3), including track length measurements, and a total of seven AHe ages (Table 4). All three systems yield middle to late Cretaceous ages. In passing the chi square test at the 5% level, all bedrock fission

Table 1. Results From Zircon Fission Track Thermochronology^a

| Sample | Latitude South (DD) | Longitude East (DD) | Dated Grains (n) | ρ_d (10^6 cm^{-2}) | N_d | Spontaneous | | Induced | | $P(\chi^2)$, (%) | ZFT (central) age (Ma) | 1σ |
|-------------------------------------------------|---------------------|---------------------|------------------|-------------------------------------|--------|-------------------------------------|--------|-------------------------------------|--------|-------------------|------------------------|-----------|
| | | | | | | ρ_s (10^6 cm^{-2}) | N_s | ρ_i (10^6 cm^{-2}) | N_i | | | |
| <i>Edwards Islands—Canisteeo Peninsula</i> | | | | | | | | | | | | |
| MB 372-2 m | -73.87633 | -103.09833 | 10 | 1.278 | (3032) | 15.793 | (1640) | 12.971 | (1347) | 56 | 103.1 | ±4.3 |
| <i>McKinzie Islands—Eastern Pine Island Bay</i> | | | | | | | | | | | | |
| MB 368-1 m | -74.04200 | -101.81817 | 10 | 1.209 | (3032) | 7.722 | (2444) | 5.918 | (1873) | 17 | 104.9 | ±4.4 |
| <i>Suchland Islands—Eastern Pine Island Bay</i> | | | | | | | | | | | | |
| MB 366-1 m | -74.11700 | -102.44633 | 4 | 1.234 | (3032) | 17.947 | (426) | 15.925 | (378) | 72 | 92.2 | ±6.8 |
| <i>Brownson Islands—Eastern Pine Island Bay</i> | | | | | | | | | | | | |
| MB 363-8 w | -74.13433 | -103.36667 | 10 | 1.251 | (3032) | 12.533 | (2008) | 10.167 | (1629) | 13 | 102.2 | ±4.7 |
| MB 392-1 m | -74.19000 | -103.57833 | 10 | 1.151 | (3032) | 25.013 | (2078) | 20.21 | (1679) | 74 | 94.5 | ±3.6 |
| <i>Backer Islands—Eastern Pine Island Bay</i> | | | | | | | | | | | | |
| MB 386-1 m | -74.35083 | -102.87400 | 10 | 1.16 | (3032) | 20.396 | (1997) | 16.811 | (1646) | 71 | 93.3 | ±3.6 |
| MB 385-1 m | -74.47317 | -102.38983 | 10 | 1.176 | (3032) | 13.603 | (2731) | 10.555 | (2119) | 18 | 101 | ±4.0 |
| MB 389-2 m | -74.52500 | -102.50833 | 10 | 1.311 | (3079) | 11.089 | (2303) | 11.007 | (2286) | 91 | 87.6 | ±3.1 |

^aZircon fission track (ZFT) data of Pine Island Bay. All analyses are by the external detector method using 0.5 for the $4\pi/2\pi$ geometry correction factor. Zircon ages calculated using dosimeter glass CN1 and zeta-CN1 = 135.1 ± 2.8 ($\pm 1\sigma$). $P(\chi^2)$ is the probability of obtaining χ^2 value for ν degrees of freedom (where ν is the number of crystals - 1) [Galbraith, 1981]; pooled ρ_s/ρ_i ratio is used to calculate age and uncertainty where $P(\chi^2) > 5\%$; mean ρ_s/ρ_i ratio is reported for samples where $P(\chi^2) < 5\%$ and for which Central ages [Galbraith and Green, 1990] are calculated.

track ages indicate that the samples are kinetically homogenous. Whenever possible, several dating methods were applied to the same sample. For the “MBL” samples all but one mean helium age has a corresponding AFT age, and eight of the “MB” samples have been dated using both AFT and ZFT. Additionally, seven of the MB samples presented here were dated earlier with zircon U/Pb geochronology (Figures 1 and 2) [Mukasa and Dalziel, 2000]. Two samples (MBL-72-10 and MBL-05-10; Tables 2 and 4) show cross-over relations of the AFT and AHe systems, with the AHe age being older than the corresponding AFT age, but they lie within associated error limits.

6.2. ZFT Results

Eight ZFT ages range between 87.6 ± 3.1 and 104.9 ± 4.4 Ma, thus consistently yielding mid-Cretaceous ages (Table 1). ZFT ages are mostly within the range of their corresponding U/Pb crystallization ages, partly even matching them within error limits (Figure 2b). Each age is based on 10 single-grain ages, except for MB 366-1 m where only four zircon grains could be dated.

6.3. AFT Results—Bedrock and IRD Samples

6.3.1. Bedrock Samples

Only two of the bedrock samples failed to provide the desired minimum number of 20 grains for AFT analysis (MB 372-2 m and MB 387-1 m; see Table 2). AFT ages range between 61.2 ± 7.8 and 120.5 ± 9.0 Ma, with a peak at ~90 Ma (Figure 2b and Table 2). Mean fission track lengths range from 13.2 to 14.9 μm with standard deviations of 0.7 to 1.4 μm (Figure S4). D_{par} values range from 1.7 to 2.5 μm (Table 2). Due to poor sample quality, limited material and in some cases rather low (<10–30 ppm) uranium concentrations, we were able to measure the desired number of 100 track lengths per sample (as recommended by Laslett et al. [1982]) in only two samples. However, for the majority of samples the track length distributions are narrow, and standard deviations are 1 μm or less for more than half of the data set (Table 2). Following Rahn and Seward [2000], who suggested that changes in standard deviation, mean length, and distribution patterns become negligible for a narrow track length distribution after a total of about 30 measurements, we base further interpretation on those samples for which there are >30 length measurements. Thus, 17 out of 25 samples were used for thermal history modeling. Even though track lengths distributions are dominantly narrow, a slight negative skew and mean track lengths of <14 μm are apparent in some samples (e.g., MB-366-1 M, MB-385-1 M, and MBL-09-10; Figure S4).

6.3.2. AFT Results for Ice Rafted Debris Samples

Based on 81 to 86 AFT single-grain ages, two age groups were identified for MBL-33 and MBL-35, with a poorly defined Jurassic to Early Cretaceous age group and a dominant late Cretaceous age group, which

Table 2. Results From Apatite Fission Track Thermochronology^a

| Sample | Latitude Sout (DD) | Longitude West (DD) | ρ^D (10^6 cm^{-2}) | ρ^S (10^6 cm^{-2}) | ρ^I (10^6 cm^{-2}) | $P(\chi^2)$ (%) | Dated grains (n) | U (ppm) | v.c. ^b of U Content (%) | AFT (Central) Age (Ma) | MTL (μm) | SE (μm) | SD (μm) | # of lengths | D_{par} Mean (μm) |
|-------------------------------------------------|--------------------|---------------------|-------------------------------------|-------------------------------------|-------------------------------------|-----------------|------------------|---------|------------------------------------|------------------------|-----------------------|----------------------|----------------------|--------------|-----------------------------------------|
| | | | | | | | | | | | | | | | |
| <i>Lindsay Islands—Canisteeo Peninsula</i> | | | | | | | | | | | | | | | |
| MBL-70-10 | -73.60202 | -103.02123 | 1.57 (11804) | 5.83 (2850) | 12.24 (728) | 95.84 (56) | 22 | 9.27 | ±22 | 116.1 | 13.6 | ±0.2 | 1.0 | (44) | 1.8 |
| MB 381-1 m | -73.61967 | -103.29033 | 1.15 (2850) | 0.26 (2850) | 0.80 (542) | 66.24 (131) | 20 | 24.84 | ±37 | 65 | 13.8 | ±0.2 | 1.4 | (57) | 1.7 |
| MB 381-2 m | -73.61967 | -103.29033 | 1.16 (2850) | 0.14 (2850) | 0.34 (131) | 99.75 (296) | 20 | 12.15 | ±83 | 84.5 | 14.2 | ±0.1 | 0.8 | (36) | 1.8 |
| <i>Edwards Islands—Canisteeo Peninsula</i> | | | | | | | | | | | | | | | |
| P569-LI-3 | -73.8528333 | 102.9888333 | 2.29 (17294) | 5.00 (2781) | 19.06 (1128) | 87.14 (83) | 19 | 10.04 | ±29 | 96.5 | - | - | - | - | 2.5 |
| MB 372-2 m | -73.87633 | -103.09833 | 1.13 (2781) | 0.80 (11804) | 2.51 (261) | 81.5 (698) | 10 | 84.22 | ±51 | 61.2 | 14.9 | ±0.2 | 0.8 | (14) | 2.3 |
| <i>Jaynes Island—Central Pine Island Bay</i> | | | | | | | | | | | | | | | |
| MBL-72-10 | -73.96933 | -104.13483 | 1.96 (11804) | 1.61 (15024) | 6.52 (2836) | 83.52 (69) | 21 | 43.59 | ±30 | 77.6 | 13.8 | ±0.1 | 1.0 | (100) | 2.3 |
| <i>McKinzie Islands—Eastern Pine Island Bay</i> | | | | | | | | | | | | | | | |
| MBL-74-10 | -74.03220 | -101.74243 | 2.03 (2900) | 0.35 (2850) | 1.26 (247) | 55.94 (139) | 20 | 7.17 | ±46 | 91.6 | 13.9 | ±0.2 | 1.1 | (37) | 1.8 |
| MB 368-1 m | -74.04200 | -101.81817 | 1.17 (2850) | 0.57 (2850) | 1.12 (272) | 98.54 (186) | 20 | 29 | ±122 | 102.1 | 13.9 | ±0.2 | 0.9 | (15) | 1.9 |
| MB 368-2 m | -74.04200 | -101.81817 | 1.18 (11804) | 0.32 (2726) | 0.87 (501) | 57.80 (367) | 20 | 26.84 | ±63 | 74.8 | 13.8 | ±0.1 | 0.8 | (32) | 1.8 |
| <i>Clark Island—Central Pine Island Bay</i> | | | | | | | | | | | | | | | |
| MBL-76-10 | -74.07300 | -105.15135 | 1.98 (2850) | 1.10 (2726) | 2.93 (972) | 25 (784) | 29 | 17.29 | ±30 | 120.5 | 13.5 | ±0.2 | 0.7 | (21) | 1.8 |
| <i>Suchland Islands—Eastern Pine Island Bay</i> | | | | | | | | | | | | | | | |
| MB 366-1 m | -74.11700 | -102.44633 | 1.19 (2850) | 1.26 (2953) | 3.33 (2074) | 33 (1169) | 20 | 99.33 | ±19 | 75.7 | 13.6 | ±0.1 | 1.0 | (66) | 1.9 |
| <i>Brownson Islands—Eastern Pine Island Bay</i> | | | | | | | | | | | | | | | |
| MB 364-1 m | -74.12833 | -103.37000 | 1.19 (2953) | 1.12 (23347) | 2.57 (2681) | 97 (87) | 20 | 88.02 | ±48 | 88.8 | 13.3 | ±0.1 | 1.0 | (82) | 2.0 |
| MBL-09-10 | -74.13368 | -103.68540 | 1.51 (2988) | 0.44 (2988) | 1.37 (271) | 15 (64) | 21 | 11.12 | ±62 | 80.1 | 11.9 | ±0.2 | 1.2 | (40) | 1.6 |
| MB 363-8 w | -74.13433 | -103.36667 | 1.21 (11804) | 0.24 (11804) | 0.73 (197) | 99 (75) | 21 | 22.02 | ±49 | 67.1 | 13.8 | ±0.2 | 1.0 | (33) | 1.6 |
| MBL-05-10 | -74.14442 | -103.36933 | 2.05 (2970) | 0.50 (2970) | 2.00 (299) | 31 (438) | 20 | 11.13 | ±62 | 83.5 | 11.6 | ±0.1 | 0.8 | (30) | 1.7 |
| MB 363-7 w | -74.16667 | -103.60000 | 1.20 (3005) | 0.42 (3005) | 0.92 (972) | 0 (204) | 20 | 29.07 | ±59 | 83.5 | 13.2 | ±0.2 | 0.9 | (36) | 1.8 |
| MB 362-3 p | -74.16667 | -103.60000 | 1.22 (2709) | 0.69 (2709) | 2.00 (586) | 36 (852) | 20 | 61.98 | ±67 | 69.6 | 13.4 | ±0.3 | 1.3 | (16) | 1.7 |
| MB 392-1 m | -74.19000 | -103.57833 | 1.10 (2726) | 1.19 (2726) | 2.49 (1787) | 51 (223) | 20 | 80.81 | ±26 | 89.1 | 13.4 | ±0.1 | 1.1 | (85) | 1.7 |
| MB 392-2 m | -74.19000 | -103.57833 | 1.10 (2726) | 1.06 (2726) | 2.45 (516) | 70 (449) | 20 | 76.88 | ±43 | 81.3 | 13.5 | ±0.2 | 0.9 | (14) | 1.8 |
| <i>Backer Islands—Eastern Pine Island Bay</i> | | | | | | | | | | | | | | | |
| MBL-14-10 | -74.33615 | -102.81238 | 2.01 (2813) | 1.05 (2779) | 3.00 (1286) | 21 (1310) | 20 | 17.74 | ±38 | 112.8 | 14.0 | ±0.1 | 0.9 | (100) | 2.2 |
| MB 386-1 m | -74.35083 | -102.87400 | 1.14 (2779) | 1.06 (2779) | 2.27 (2795) | 8 (28) | 20 | 69.73 | ±17 | 92.2 | 14.1 | ±0.1 | 0.9 | (83) | 2.1 |
| MB 387-1 m | -74.42333 | -102.48167 | 1.12 (2831) | 0.17 (2831) | 0.46 (78) | 55 (534) | 6 | 42.11 | ±202 | 68.9 | 15.3 | ±0.6 | 1.1 | (3) | n.a. |
| MB 385-1 m | -74.47317 | -102.38983 | 1.15 (2744) | 0.74 (2744) | 1.50 (1077) | 65 (217) | 20 | 46.31 | ±20 | 96.8 | 13.9 | ±0.1 | 0.9 | (87) | 2.0 |
| MB 389-2 m | -74.52500 | -102.50833 | 1.11 (2761) | 0.67 (2761) | 1.58 (511) | 91 (724) | 20 | 51.05 | ±74 | 80.5 | 14.2 | ±0.2 | 0.9 | (26) | 1.7 |
| MB 389-1 m | -74.52500 | -102.50833 | 1.12 (2761) | 0.84 (2761) | 2.08 (1796) | 45 (449) | 20 | 65.49 | ±52 | 76.9 | 13.6 | ±0.1 | 1.0 | (62) | 1.9 |

^aApatite fission track (AFT) data of Pine Island Bay, AFT ages were determined by counting spontaneous and induced fission tracks according to the Zeta (ζ) calibration method [Hurford and Green, 1982, 1983; Green, 1985]; ρ^D , ρ^S , ρ^I , N_d , N_s , N_i ; density and number of counted dosimeter, spontaneous, and induced tracks; $P(\chi^2)$; χ^2 probability. All apatite fission track analyses were done by the external detector method using SRM612 dosimeter glasses for MB samples and CNS dosimeter glasses for MBL and "P569" samples. Zeta (ζ) values for MBL and P569 samples are 324 ± 11 (Lindow) and for MB 344 ± 5 (JL). All mounts were etched with 5 M HNO₃ at 20°C for 20 s, and correspondent mica plates were etched with 40% HF at 20°C for 30 min. Diameter of etched spontaneous fission tracks (D_{par}) was measured for investigated grains as a proxy of track annealing kinetic properties [e.g., Donelick, 1993; Carlson et al., 1999]. AFT ages were calculated using program Trackkey [Dunkl, 2002]. Errors are quoted as $\pm 1\sigma$ [Green, 1981]. If possible, 100 fission track lengths for each sample were measured following the recommendations of Laslett et al. [1982]. Mean track length (MTL) and standard deviation (SD) are quoted for all samples where fission track lengths were measured.

^bv.c. stands for "coefficient of variation," the ratio of the standard deviation to the mean.

Table 3. AFT Analysis and Binomial Peak Fitting of IRD Samples^a

| Sample (Coring Sites on Cruise ANT-XXV/3) | Latitude South (DD) | Longitude West (DD) | Elevation (m) | Dated Gains (n) | ρ^d (10^6 cm^{-2}) | ρ^s (10^6 cm^{-2}) | ρ^i (10^6 cm^{-2}) | $P(\chi^2)$ | | U (ppm) | v.c. ^b of U Content (%) | AFT (Central) age (Ma) | 1 σ |
|-------------------------------------------|------------------------|---------------------|-------------------|-------------------------|-------------------------------------|-------------------------------------|-------------------------------------|-------------------|-------------------|---------|------------------------------------|------------------------|------------|
| | | | | | | | | (N _d) | (N _i) | | | | |
| MBL-33-10 [PS75/192-2] | -71.74483 | -103.32683 | -793 | 81 | 1.55 (23347) | 0.94 | (786) | 2.85 | (2389) | 0.00 | na | na | 6 |
| | AFT age peak 1 (Ma) 62 | ± (Ma) | Peak size (%) 54 | AFT age peak 2 (Ma) 113 | | | | | | | | | |
| MBL-34-10 [PS75/215-1] | -74.59183 | -104.04183 | -556 | 81 | 1.52 (23347) | 2.66 | (2937) | 7.90 | (8715) | 11.22 | 60 | ±39 | 83 |
| | AFT age peak 1 (Ma) 84 | ± (Ma) | Peak size (%) 100 | AFT age peak 2 (Ma) - | | | | | | | | | |
| MBL-35-10 (A) [PS75/219-2] | -73.66667 | -108.99933 | -461 | 86 | 1.53 (23347) | 0.63 | (1002) | 1.92 | (3066) | 0.00 | 17 | ±110 | 92 |
| | AFT age peak 1 (Ma) 69 | ± (Ma) | Peak size (%) 75 | AFT age peak 2 (Ma) 196 | | | | | | | | | |

^aApatite fission track analyses were done by the external detector method using CNS dosimeter glasses and Zeta (Z) values are 324 ± 11 (Lindow). All mounts were etched with 5 M HNO₃ at 20°C for 20 s, and correspondent mica plates were etched with 40% HF at 20°C for 30 min (see supporting information S1 for detailed single-grain age listing).
^bv.c. stands for "coefficient of variation," the ratio of the standard deviation to the mean.

Table 4. Results From Apatite (U-Th-Sm)/He Thermochronology^a

| Sample | Latitude South (DD) | Longitude East (DD) | Elevation (m) | Aliquot ^b | Mean Radius (μm) | Sm ¹⁴⁷ (ppm) | Th ²³² (ppm) | U ²³⁸ + ²³⁵ U (ppm) | ⁴ He (ncc) | Th/U | eU ^c (ppm) | Uncorrected Age | | Corrected Age | | AHe (mean) age (Ma) | SE (Ma) | SD (Ma) | |
|-------------------------------------------------|---------------------|---------------------|---------------|----------------------|------------------|-------------------------|-------------------------|-------------------------------------------|-----------------------|--------|-----------------------|-----------------|--------------|-------------------------------------------|--------------|---------------------|---------|---------|--|
| | | | | | | | | | | | | Age (Ma) | ± Error (Ma) | Weighted F _t ^d (Ma) | ± Error (Ma) | | | | |
| <i>Edwards Islands—Caniesto Peninsula</i> | | | | | | | | | | | | | | | | | | | |
| MBL-70-10 | -73.60202 | -103.02123 | 29 | ap1 ^e | 43.7 | 29.529 | 22.449 | 5.979 | 0.120 | 3.755 | 11.216 | 76.4 | ±4.7 | 1.00 | 76.4 | ±4.7 | ±4.7 | - | |
| MBL-70-10 | -73.60202 | -103.02123 | 29 | ap2 | 102.1 | 53.829 | 27.360 | 10.503 | 2.459 | 2.605 | 16.904 | 103.5 | ±6.4 | 0.86 | 120.8 | ±14.2 | ±14.2 | - | |
| PS69-LI-3 | -73.85283 | -102.98883 | 5 | ap1 ^b | 38.3 | 42.837 | 69.221 | 21.507 | 0.925 | 3.218 | 37.609 | 43.7 | ±2.7 | 0.71 | 61.4 | ±7.2 | ±4.5 | ±8.9 | |
| PS69-LI-3 | -73.85283 | -102.98883 | 5 | ap2 ^b | 37.4 | 70.324 | 63.590 | 13.637 | 0.740 | 4.663 | 28.460 | 45.9 | ±2.8 | 0.65 | 70.4 | ±8.3 | ±8.3 | - | |
| PS69-LI-3 | -73.85283 | -102.98883 | 5 | ap3 ^b | 35.4 | 51.096 | 46.980 | 9.109 | 0.402 | 5.157 | 20.060 | 40.1 | ±2.5 | 0.63 | 63.7 | ±7.5 | ±7.5 | - | |
| PS69-LI-2 | -73.85283 | -102.98883 | 5 | ap1 ^b | 69.1 | 52.561 | 47.117 | 10.188 | 3.618 | 4.624 | 21.172 | 55.7 | ±3.5 | 0.80 | 69.5 | ±8.2 | ±8.2 | - | |
| <i>Jaynes Island—Central Pine Island Bay</i> | | | | | | | | | | | | | | | | | | | |
| MBL-72-10 | -73.96933 | -104.13483 | 17 | ap1 | 63.9 | 17.983 | 140.484 | 81.136 | 4.174 | 1.731 | 113.746 | 58.8 | ±3.6 | 0.79 | 73.9 | ±8.7 | ±6.0 | ±10.4 | |
| MBL-72-10 | -73.96933 | -104.13483 | 17 | ap2 | 51.4 | 13.533 | 77.974 | 44.966 | 2.213 | 1.734 | 63.069 | 61.6 | ±3.8 | 0.74 | 83.2 | ±9.8 | ±9.8 | - | |
| MBL-72-10 | -73.96933 | -104.13483 | 17 | ap3 | 43.5 | 16.185 | 103.588 | 64.328 | 1.310 | 1.610 | 88.377 | 53.7 | ±3.3 | 0.68 | 78.9 | ±9.3 | ±9.3 | - | |
| <i>McKinzie Islands—Eastern Pine Island Bay</i> | | | | | | | | | | | | | | | | | | | |
| MBL-74-10 | -74.03220 | -101.74243 | 13 | ap1 | 93.2 | 10.621 | 10.550 | 2.798 | 0.735 | 3.771 | 5.256 | 53.6 | ±3.3 | 0.85 | 62.8 | ±7.4 | ±14.4 | ±20.3 | |
| MBL-74-10 | -74.03220 | -101.74243 | 13 | ap2 | 67.9 | 33.866 | 42.497 | 6.136 | 0.604 | 6.925 | 16.029 | 66.4 | ±4.1 | 0.75 | 88.6 | ±10.4 | ±10.4 | - | |
| MBL-74-10 | -74.03220 | -101.74243 | 13 | ap3 | 39.6 | 23.039 | 48.446 | 1.097 | 0.253 | 44.160 | 12.360 | 92.3 | ±5.7 | 0.65 | 141.7 | ±16.7 | ±16.7 | - | |
| <i>Clark Island—Central Pine Island Bay</i> | | | | | | | | | | | | | | | | | | | |
| MBL-76-10 | -74.07300 | -105.15135 | 4 | ap1 | 50.3 | 2.422 | 4.614 | 6.591 | 0.190 | 0.700 | 7.664 | 67.0 | ±4.2 | 0.72 | 93.4 | ±11.0 | ±7.8 | ±11.0 | |
| MBL-76-10 | -74.07300 | -105.15135 | 4 | ap2 | 48.6 | 25.944 | 5.689 | 17.921 | 0.694 | 0.317 | 19.266 | 83.4 | ±5.2 | 0.72 | 115.4 | ±13.6 | ±13.6 | - | |
| MBL-76-10 | -74.07300 | -105.15135 | 4 | ap3 | 66.7 | 18.770 | 2.266 | 10.979 | 0.613 | 0.206 | 11.523 | 75.3 | ±4.7 | 0.81 | 93.6 | ±11.0 | ±11.0 | - | |
| <i>Brownson Islands—Eastern Pine Island Bay</i> | | | | | | | | | | | | | | | | | | | |
| MBL-05-10 | -74.14442 | -103.36933 | 13 | ap2 | 29.7 | 39.530 | 16.620 | 7.579 | 0.083 | 2.193 | 11.474 | 76.8 | ±4.8 | 0.53 | 143.7 | ±16.9 | ±7.6 | ±10.8 | |
| MBL-05-10 | -74.14442 | -103.36933 | 13 | ap3 | 27.4 | 62.330 | 30.630 | 10.978 | 0.105 | 2.790 | 18.146 | 50.7 | ±3.1 | 0.56 | 91.0 | ±10.7 | ±10.7 | - | |
| MBL-05-10 | -74.14442 | -103.36933 | 13 | ap4 | 38.0 | 103.116 | 54.941 | 18.933 | 0.218 | 2.902 | 31.783 | 56.7 | ±3.5 | 0.65 | 87.7 | ±10.3 | ±10.3 | - | |
| <i>Backer Islands—Eastern Pine Island Bay</i> | | | | | | | | | | | | | | | | | | | |
| MBL-14-10 | -74.33615 | -102.81238 | 17 | ap1 | 44.3 | 49.488 | 118.797 | 23.651 | 1.681 | 5.023 | 51.261 | 63.9 | ±4.0 | 0.71 | 90.1 | ±10.6 | ±5.3 | ±10.6 | |
| MBL-14-10 | -74.33615 | -102.81238 | 17 | ap2 | 43.4 | 55.096 | 102.673 | 26.130 | 0.872 | 3.929 | 50.005 | 59.6 | ±3.7 | 0.68 | 87.8 | ±10.3 | ±10.3 | - | |
| MBL-14-10 | -74.33615 | -102.81238 | 17 | ap3 | 76.3 | 40.647 | 88.344 | 18.328 | 6.449 | 4.820 | 38.864 | 73.2 | ±4.5 | 0.83 | 88.5 | ±10.4 | ±10.4 | - | |
| MBL-14-10 | -74.33615 | -102.81238 | 17 | ap4 | 56.7 | 41.718 | 70.299 | 15.083 | 1.549 | 4.661 | 31.434 | 68.6 | ±4.3 | 0.76 | 90.5 | ±10.7 | ±10.7 | - | |

^aApatite helium (AHe) data of Pine Island Bay; "SD" stands for standard deviation and "SE" is the standard error of the calculated mean age, as for being older (within the error) than their corresponding AFT age.

^bMultigrain aliquot of three crystals.

^cEffective uranium concentration, calculated as U + 0.232Th + 0.001Sm (adopted for Sm from Shuster et al. [2006]).

^dα_e ejection correction after Farley et al. [1996], weighted according to the measured mother-isotope concentration.

^eAbraded grain.

shows in all samples (Table 3). The F test for a three-peak (or more) solution fails. Thus, although the dated clasts are presumably at least partly derived from deeper incised areas as compared to samples from islands in Pine Island Bay, no younger, post-Cretaceous AFT age group occurs in the IRD samples. Instead, the detrital age groups are similar to those obtained from bedrock exposures in Pine Island Bay or are even older. Here the results mostly represent erosion of granitoid source rocks, whereas erosion of Cenozoic volcanogenic rocks from the area is not monitored. This is because the volcanogenic rocks have very poor abundance or are even completely devoid of apatite, a finding that was also corroborated by thin section analysis of the volcanogenic clasts.

6.4. AHe Results

AHe mean ages derived from seven samples range between 66 ± 9 and 94 ± 11 Ma (Figure 2b and Table 4). For seven samples, AHe dating was carried out on single apatite grain aliquots, with no less than two and a maximum of four aliquots for each sample (Table 4). Only sample PS69 was dated through multigrain aliquots. This was the first AHe sample analyzed in Pine Island Bay, so we had no prior knowledge of the helium age it would yield. To ensure sufficient helium yield, even in case of rather young AHe ages (e.g., less than 5 Ma), we chose the multigrain aliquot approach. Sample MBL-70-10 only comprises two single-grain aliquots, and one of the two apatite grains was mechanically abraded prior to Helium outgassing (Table 4). Mechanical abrasion is an option to remove the crystal's outer rim [Spiegel *et al.*, 2009] to avoid the need for corrections for He loss at the grain margin (alpha ejection correction, see supporting information). In case of MBL-70-10, abrasion was used to date a big apatite fragment ($\sim 220 \mu\text{m}$ in diameter), which could not be corrected for alpha ejection because of its irregular morphology. However, the two results for MBL-70-10 show the biggest variance in AHe ages, with 76.4 ± 4.7 and 120.8 ± 14.2 Ma (Table 4). The older aliquot, and also some aliquots of other samples, yielded ages that are older than the corresponding AFT ages within their error. We explain these differences as being due to the presence of tiny U-Th bearing inclusions such as zircon or monazite, too small to be detected by microscopic observations. The "too old" aliquots are included in Table 4 but are excluded from further interpretation. For the rest of the aliquots, AHe ages of one sample agree within error limits, which is why we calculated and use the arithmetic means. These range between 66 and 94 Ma (Table 4).

6.5. Thermal History Modeling

All models are characterized by two main cooling trends: (i) very rapid to almost instantaneous Cretaceous cooling (e.g., $\sim 900^\circ\text{C}$ in less than 20 Myr; MBL-70-10) and (ii) late Cretaceous/Cenozoic very slow cooling (Figure 4). However, some samples (e.g., MBL-14-10) may show a shift to a phase of marked cooling since approximately 10 Ma (Figure S5). Finally, not all samples would provide model solutions based on the whole data set. Particularly, samples with single-grain AHe ages not overlapping within their errors had to be modeled individually. This relates particularly to sample MBL-74-10 (Table 4). In the end, the single-grain models from the same sample show almost identical slopes and weighted mean paths for their cooling histories (Figure S5).

7. Discussion

7.1. Cretaceous-Cenozoic Geodynamics—Cooling, Exhumation, and Tectonic Denudation

7.1.1. Potential Relationship Between Cooling and Exhumation

Dating of bedrock and detrital sediments shows that all samples are dominated by Cretaceous ages, indicating minimal net denudation during the Cenozoic. This is corroborated by thermal history modeling, which shows that sample host rocks experienced rapid cooling to shallow crustal levels during the Cretaceous. Generally, cooling rates can be converted into exhumation rates by assuming a reasonable geothermal gradient. For the case of West Antarctica, however, this approach is problematic. The difficulties hereby arise from the extensional setting and strong magmatic activity during the Cretaceous, which suggest an enhanced geothermal gradient ($40\text{--}70^\circ\text{C}/\text{km}$) in that area and strong variation in heat flux through space and time. Thermobarometry data from hornblendes in Pine Island Bay granitoids indicate a geothermal gradient of $60\text{--}65^\circ\text{C}/\text{km}$ for the early Cretaceous [Mehling, 2015]. Moreover, the observed cooling may not be related to dynamic exhumation; rather, it may result from static isotherm relaxation after a period of magmatic intrusion. Combining regional geology with thermochronology may nevertheless allow for an estimate of Cretaceous exhumation along Pine Island Bay and the adjacent coasts of eastern Amundsen Sea

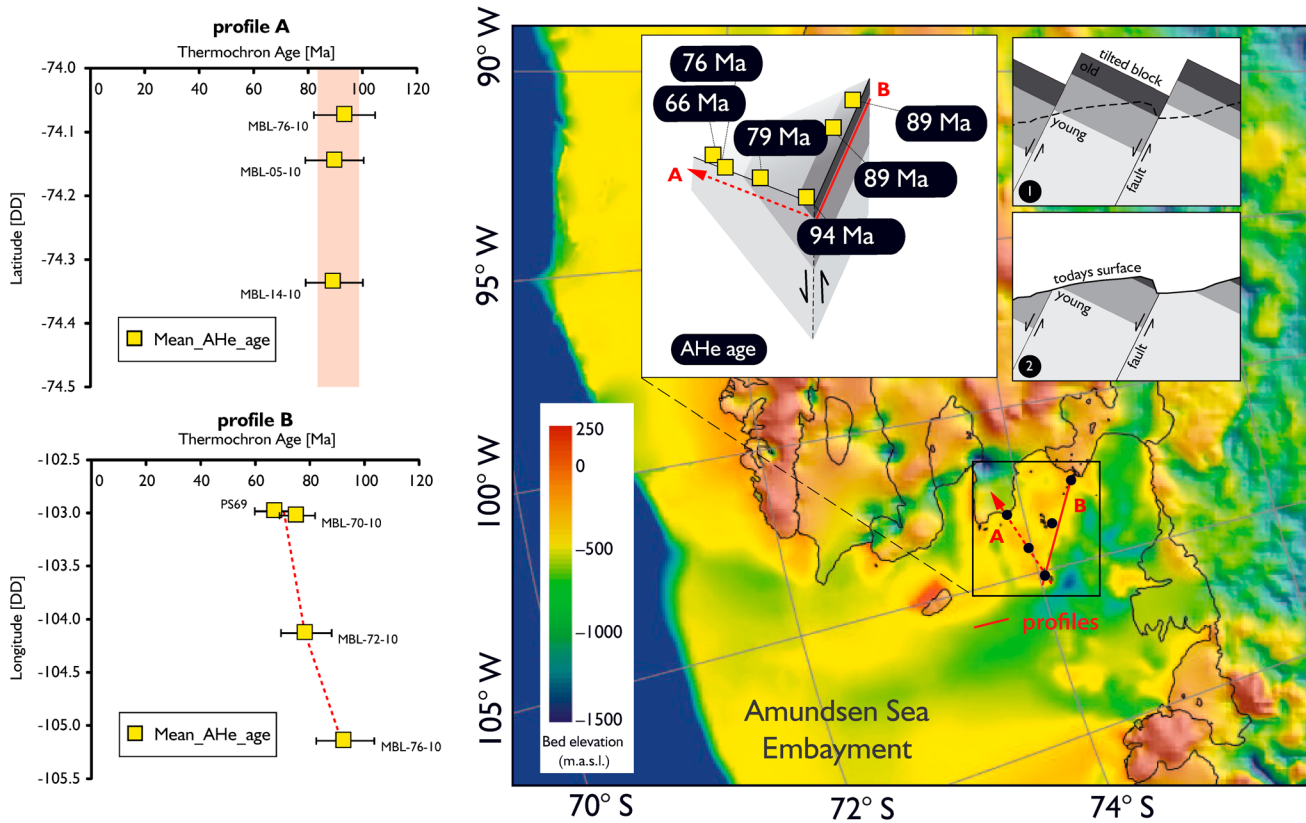


Figure 3. Age-location plots of mean apatite (U-Th-Sm)/He ages (Ma) from Pine Island Bay. (top left) Bay-parallel profile A. (bottom left) Bay-normal profile B. (right) AHe age distribution in map view and schematic illustration of crustal tilting. Underlying topographic map from *Bingham et al.* [2012].

Embayment. Some of the granitoid rocks of Pine Island Bay intruded as late as 96 to 94 Ma, having reached temperatures of 40 to 50°C by ~75–60 Ma. Even if isotherm relaxation plays a dominant role, these temperatures can only be reached after magmatic bodies were exhumed to shallow crustal levels of 1 to 2 km (1 km seems even more likely, given that the geothermal gradient was presumably still enhanced). Assuming shallow emplacement depths of 5 to 10 km, similar to magmatic bodies in the Alps and Himalaya, this would suggest regional late Cretaceous exhumation rates in the range 0.08 to 0.47 km/Myr. For the early Cretaceous of Pine Island Bay the results of *Mehling, 2015* indicate an intrusion depth of 11 km which would translate into early Cretaceous to Cenozoic exhumation rates of 0.11 to 0.13 km/Myr.

7.1.2. Erosion Versus Tectonic Denudation: Reconciling Exhumation With the Sedimentary Record

Since ~100 Ma, the Amundsen Sea Embayment of West Antarctica was dominated by extension. Thus, a question arises whether or not the estimated exhumation rates result from erosion or rather from tectonic denudation caused by normal faulting. Unlike tectonic denudation, erosional denudation is associated with sediment production. In addressing this question, we tried to reconcile sediment volumes presumably derived from the Amundsen Sea margin with the exhumation history extracted from thermochronology. The combined catchment area of glaciers draining into the Amundsen Sea, i.e., of Pine Island, Thwaites, Smith, and Kohler glaciers, including adjacent ice streams, is about $0.4 \times 10^6 \text{ km}^2$ [*Rignot et al., 2008*]. The eastern Amundsen Sea area in turn accommodates a shelf area plus continental rise of approximately $1.7 \times 10^6 \text{ km}^2$ [*Wobbe et al., 2014*] with sediment thicknesses ranging between ~1 and 0.2 km from isolated thin basins beneath or near the Pine Island ice shelf [*Muto et al., 2013; Nitsche et al., 2013*], up to 7 km on the middle shelf and thinning to 3–4 km toward the continental shelf edge [*Gohl et al., 2013b*]. The total sediment volume estimates for the eastern Amundsen Sea area are about $1.8 \times 10^6 \text{ km}^3$ with an average marine sediment cover of ~1 km [*Wobbe et al., 2014*]. If net exhumation of ~7 km is assumed (based on an assumed emplacement depth of >7 km and an average enhanced geothermal gradient of 50°C/km since the mid-Cretaceous), and all exhumation was transferred into erosion, then, for the combined drainage area of Pine Island Glacier and Thwaites Glacier (which has to be assumed the same since the Cretaceous), a sediment

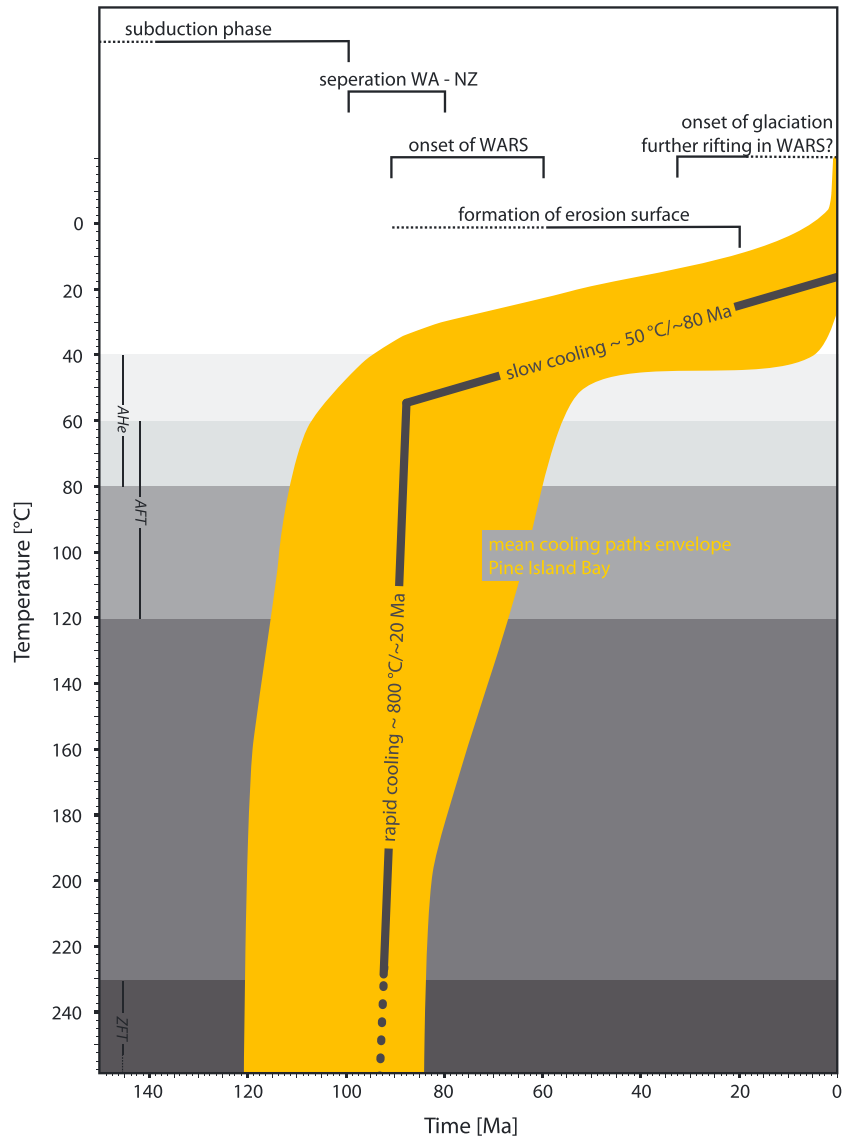


Figure 4. Sketch showing in orange the weighted mean path envelope of the modeled time-temperature paths for sample host rocks in Pine Island Bay, West Antarctica. Dark gray bold lines indicate the dominant cooling pattern and average cooling rates. Above is the timing of major tectonic events affecting the Amundsen Sea area and West Antarctica. Abbreviations: WARS = West Antarctic Rift System, WA = West Antarctica, NZ = New Zealand. Grey shading refers to the temperature sensitivities of the zircon and apatite fission track, and (U-Th-Sm)/He systems and to the overlap of the temperature sensitivities.

load of $2.9 \times 10^6 \text{ km}^3$ would result. This is more than the eastern Amundsen shelf area alone could account for (based on the above sediment volume estimate $1.8 \times 10^6 \text{ km}^3$). Other potential sediment sinks, apart from the Amundsen shelf, are (i) the rift basins of the West Antarctic Rift System, i.e., a landward sediment sink; or (ii) a sink on the Zealandia side prior to and during mid-Cretaceous extension and separation of Zealandia crustal blocks from West Antarctica. However, most of the Cretaceous sediment preserved in the New Zealand region occurs in the forearc region and can be related to uplift and erosion of the inboard region of the accretionary wedge, so there is no indication of massive Cretaceous sediment layers on the other side of the continental rift. In summary, the mismatch between the thickness of preserved strata (as far as it is known) and the thickness of material removed from bedrock exposures based on our Cretaceous to Cenozoic exhumation estimates of 0.08 to 0.47 km/Myr suggests that tectonic denudation played a role in exhuming basement in the coastal area around the eastern Amundsen Sea, although of course the huge errors associated with the sediment budget calculation need to be kept in mind.

7.1.3. Trigger Mechanisms of Cretaceous Denudation

The exact timing of the onset of rapid cooling and denudation cannot be determined from our thermochronology data because all of the sample age data are reset. Some of the analyzed samples do, however, record rapid cooling as early as 120 Ma. A similar timing has been identified by *Welke et al.* [2016] in the Ross Sea embayment of West Antarctica from zircon helium dating of detrital samples, which show a dominant age population of 180 to 130 Ma. Based on that, *Welke et al.* [2016] infer a Gondwana breakup related exhumation event for this section of the Transantarctic Mountains. At that time, the Zealandia crustal blocks (including Campbell Plateau, Chatham Rise, North Island, and South Island; Figure S1) were still contiguous with West Antarctica and subduction of Phoenix Plate beneath the eastern Gondwana margin was still ongoing. It seems reasonable to assume that during the early Cretaceous, the area, being affected by long-term crustal convergence and magmatic activity, was characterized by thickened crust and pronounced topographic relief, probably similar to the present-day Andes orogen. Rapid cooling and exhumation is consistent with this scenario and was presumably related to tectonic uplift and erosion. At about 100–94 Ma, convergence ceased, possibly a result of collision of Hikurangi Plateau with the subduction margin [*Mukasa and Dalziel*, 2000; *Davy et al.*, 2008], and between 90 and 84 Ma, the first oceanic crust was formed between Zealandia crustal blocks and West Antarctica [e.g., *Eagles et al.*, 2004; *Wobbe et al.*, 2012], leaving West Antarctica as a passive margin. For most of the samples, however, rapid cooling and exhumation continued during the late Cretaceous, partly until ~60 Ma and younger, at rates which are unusually high for passive margin settings. A scenario which convincingly explains the high cooling rates, tectonic denudation and the overall geological setting, involves gravitational collapse of the orogeny due to the development of an unsupported seaward boundary following the cessation of subduction (in the sense of *Rey et al.* [2001]). Arguments in support of such a scenario include: (i) a presumably strongly overthickened crust, resulting from >150 Myr of subduction and magmatic activity; (ii) thermal weakening of the lower to middle crust, resulting from strong magmatic activity, particularly during the Cretaceous; and (iii) rapid reduction of topography. While high-standing topography can be assumed until ~100 Ma, mean surface elevation must have been strongly reduced by ~85 Ma, following the reasoning of *LeMasurier and Landis* [1996] about the development of a widespread erosion surface across West Antarctica, which had formed at sea level by ~85 Ma. This rather rapid shift of highly elevated orogenic terrain to a low-lying landscape (close to sea level) shows all of the characteristics of an orogenic collapse. A further factor in support of late Cretaceous gravitational collapse is the unique situation of a very rapid change from convergence to extension [*Mukasa and Dalziel*, 2000; *Davy et al.*, 2008] associated with both the separation of West Antarctica from Zealandia (Pacific rifting) and of East Antarctica from West Antarctica (West Antarctic Rift System), thus providing space for collapse of previously overthickened crust.

7.2. Cenozoic Geodynamics—Rifting and Glacial Erosion?

7.2.1. Cenozoic Tectonics

Basically, all samples follow the same cooling pattern: rapid cooling during the Cretaceous shifting to less rapid cooling during the Cenozoic (Figure 4). However, the exact timing of the onset of rapid cooling and/or the shift toward slow cooling varies between individual samples from ~100 Ma to 50 Ma, with no apparent relation to the geographical positions of samples (Figure S5). We explain this spatial variance by rift-induced block faulting, juxtaposing rocks that were at slightly different crustal depths at the time of closure of the ZFT and AFT systems. This explanation is also in agreement with the fragmented bathymetry underlying Pine Island Bay (Figures 2 and 3), typically consisting of deeply incised valleys (on average at least ~500 m deep) separating island groups. However, unlike AFT and ZFT ages, AHe ages show a relationship between age and geographical position through a younging trend from 94 Ma (MBL-76-10) to 66 Ma (PS69-Li) across the bay toward the east and constant ages of ~90 Ma along Pine Island Trough (Figure 3). This pattern can best be explained by large-scale crustal tilting toward Pine Island Glacial Trough as a result of stress relief in response to crustal extension of basement within Pine Island Bay. Tilting must have occurred after the AHe system entered the PRZ (i.e., post-66 Ma) and was associated with little erosion, so that the AHe system was persevered and does not reflect posttilting exhumation (Figure 3). Basement tilting toward Pine Island Trough suggests that (i) the deeply incised Pine Island Trough indeed follows a tectonic structure [e.g., *Jordan et al.*, 2010; *Gohl et al.*, 2013a, 2013b] and (ii) that this structure was active during post-Cretaceous times. Thus, our data support the idea of Pine Island Trough being a branch of the West Antarctic Rift System connecting Amundsen Sea with the continental interior (and related consequences regarding penetration of warm sea water beneath the West Antarctic Ice Sheet) and also provide the first direct indications of

Cenozoic activity of this rift branch [e.g., *Jordan et al.*, 2010; *Gohl et al.*, 2013a, 2013b; *Warner and Roberts*, 2013; *Favier et al.*, 2014; *Mouginot et al.*, 2014].

7.2.2. Erosional Response to Glaciation

Glaciation of West Antarctica is considered to have commenced at the Eocene-Oligocene boundary [*Wilson et al.*, 2013], that is, during a time when climate was generally warmer than today. Thus, unlike most present-day polar glaciers, the ice may have not been frozen to its bed, creating a more erosive regime than that of present-day polar glaciers. Thus, one would expect that early continental glaciation caused enhanced erosion, monitored at least by the AHe system, similar to that which is described for Alaska [*Berger and Spotilla*, 2008]. Such a scenario would also be consistent with West Antarctic topography having been much higher at the Eocene-Oligocene transition than today, as suggested by *Wilson et al.* [2012]. However, AHe ages from this study show that net denudation along the eastern Amundsen Sea coast was not sufficient to completely reset the AHe system during the entire Cenozoic (which requires removing >2 to 4 km of overburden, depending on the geothermal gradient ranging somewhere between 60 to 20°C/km) and modeled thermal histories extracted from the data give no indications for any changes at the Eocene-Oligocene boundary. Therefore, based on the present data, we suggest that glacial erosion was limited and that the present-day basement morphology around Pine Island Bay and its adjoining coasts, basically results from the Cretaceous, contradicting the suggestions made by *Wilson et al.* [2012].

Thermal history inversions for most of the samples exhibit recent accelerated cooling. However, this change from slow to rapid cooling occurs at temperatures $<40^{\circ}\text{C}$, outside the temperature range where the AFT and AHe thermochronometers are most sensitive. Therefore, we are hesitant about providing an explanation for this “cooling event.” On the other hand, previous studies have shown that modern annealing algorithms do not produce young cooling events as modeling artifacts and that the AFT system is capable of monitoring thermal histories even at temperatures cooler than the top of the nominal partial annealing zone [*Spiegel et al.*, 2007]. One potential explanation would be an erosional response to isostatic uplift resulting from recent ice loss, currently reaching uplift rates of >20 mm/yr for the Amundsen Sea coast [*Groh et al.*, 2012]. However, in order to explain the cooling signal observed from our data, similar uplift rates must have persisted over the last $\sim 50,000$ yrs, and furthermore, uplift must have been balanced by erosion. Prerequisites for both of these behaviors seem unlikely.

8. Conclusion

We present the first low-temperature thermochronology results for Pine Island Bay and its adjoining coasts, West Antarctica, combined with petrographic analysis of prevalent subglacially derived clasts from the Amundsen Sea margin. Our data show that the batholithic belt comprising basement of the numerous islands in Pine Island Bay extends farther inland beneath the catchments of Pine Island and Thwaites glaciers and that the batholithic rocks were most likely intruded into low-grade metamorphic rocks. All analyzed rocks, of either island exposures or detritus from the catchments of Pine Island Glacier, Thwaites Glacier, and the Abbot Ice Shelf, show exclusively Cretaceous ages for the applied dating systems (e.g., zircon and apatite fission track, apatite (U-Th-Sm)/He thermochronology for bedrock, and apatite fission track for sediment samples). Thermal history modeling has revealed that the eastern Amundsen Sea area of coastal West Antarctica experienced rapid Cretaceous and slow Cenozoic cooling (Figure 4).

Rapid Cretaceous cooling occurred at the same rates across the transition from active margin to a passive margin tectonics along the Amundsen Sea area and was dominantly related to tectonic denudation. During the late Cretaceous/early Cenozoic, rapid reduction in mean surface elevation along the former active margin is evidenced by the development of the West Antarctic erosion surface [*LeMasurier and Landis*, 1996]. This rapid change from strong relief to a low-lying landscape (at or close to sea level) suggests that the area experienced free-boundary gravitational collapse following the end of subduction. Cenozoic tectonics, as monitored by our thermochronology data, is expressed by crustal tilting within eastern Pine Island Bay, implying that Pine Island Trough represents a branch of the West Antarctic Rift System active during the Cenozoic and connecting eastern Amundsen Sea with the continental interior of West Antarctica. At the end of the Cretaceous, rapid cooling ceased, and practically all sample host rocks had cooled to ambient temperatures below 60 to 50°C, indicating net denudation of about 3 km or less for the entire Cenozoic. These low denudation rates suggest that the Pine Island Bay area was neither affected by pervasive tectonic

activity post-Cretaceous nor did climate changes during the Cenozoic led to strongly enhanced erosion. This latter point is not consistent with reconstructions made by [Wilson *et al.*, 2012]. More research activity is required to ultimately reconcile the offshore sedimentary record imaged geophysically with thermochronological studies of rocks exposed on land.

Acknowledgments

We thank Friederike Bauer and Massimiliano Zattin for their very constructive and helpful reviews. For sampling assistance, we thank captain Uwe Pahl and the crew of RV *Polarstern* cruise ANT-XXVI/3 and the team from Heli Service International, J. Smith, I. MacNab (British Antarctic Survey), M. Scheinert, and R. Rosenau (University of Dresden). For their help with sample processing and analysis we acknowledge A. Toltz (University of Bremen) and her team of student assistants. B. Kohn (University of Melbourne) is thanked for his support regarding apatite (U-Th-Sm)/He analyses. This work was financially supported by the Deutsche Forschungsgemeinschaft (DFG) in the framework of the priority program "Antarctic Research with comparative investigations in Arctic ice areas" through grant SP673/6-1. P.J.J. Kamp acknowledges technical assistance from Xu Ganqing in the UoW lab, the provision of samples by John Bradshaw and Steve Weaver (University of Canterbury), New Zealand Government funding support (MBIE contract UOWX1501), and AINSE funding support for irradiations at ANSTO, Lucas Heights, Australia. All data used are documented in the listed references, tables, and supporting information.

References

- Bamber, J. L., R. E. M. Riva, B. L. A. Vermeersen, and A. M. LeBrocq (2009), Reassessment of the potential sea-level rise from a collapse of the West Antarctic ice sheet, *Science*, 324(5929), 901–903.
- Berger, A. L., and J. A. Spotila (2008), Denudation and deformation in a glaciated orogenic wedge: The St. Elias orogen, Alaska, *Geology*, 36(7), 523–526.
- Bingham, R. G., F. Ferraccioli, E. C. King, R. D. Larter, H. D. Pritchard, A. M. Smith, and D. G. Vaughan (2012), Inland thinning of West Antarctic Ice Sheet steered along subglacial rifts, *Nature*, 487(7408), 468–471.
- Brabander, D. J., and B. J. Giletti (1995), Strontium diffusion kinetics in amphiboles and significance to thermal history determinations, *Geochim. Cosmochim. Acta*, 59(11), 2223–2238.
- Brandon, M. T. (1992), Decomposition of fission-track grain-age distributions, *Am. J. Sci.*, 292(8), 535–564.
- Brandon, M. T. (1996), Probability density plot for fission-track grain-age samples, *Radiat. Meas.*, 26(5), 663–676.
- Brandon, M. T. (2002), Decomposition of mixed grain age distributions using BINOMFIT, *On Track*, 24, 13–18.
- Burtner, R. L., A. Nigrini, and R. A. Donelick (1994), Thermochronology of Lower Cretaceous source rocks in the Idaho-Wyoming thrust belt, *AAPG Bull.*, 78(10), 1613–1636.
- Carlson, W. D., R. A. Donelick, and R. A. Ketcham (1999), Variability of apatite fission-track annealing kinetics: I. Experimental results, *Am. Mineral.*, 84(9), 1213–1223.
- Chaput, J., R. C. Aster, A. Huerta, X. Sun, A. Lloyd, D. Wiens, A. Nyblade, S. Anandakrishnan, J. P. Winberry, and T. Wilson (2014), The crustal thickness of West Antarctica, *J. Geophys. Res. Solid Earth*, 119, 378–395, doi:10.1002/2013JB010642.
- Cherniak, D. J. (1993), Lead diffusion in titanite and preliminary results on the effects of radiation damage on Pb transport, *Chem. Geol.*, 110(1–3), 177–194.
- Dalziel, I. W. D. (2006), On the extent of the active West Antarctic rift system, paper presented at Workshop on Frontiers and Opportunities in Antarctic Geosciences, Terra Antarct. Publ., Siena, Italy.
- Dalziel, I. W. D., and D. H. Elliot (1982), West Antarctica: Problem child of Gondwanaland, *Tectonics*, 1, 3–19, doi:10.1029/TC001i001p00003.
- Dalziel, I. W. D., and L. A. Lawver (2001), The lithospheric setting of the west antarctic ice sheet, in *Antarctic Research Series*, edited by R. Bindshadler, pp. 29–44, AGU, Washington, D. C.
- Davy, B., K. Hoernle, and R. Werner (2008), Hikurangi Plateau: Crustal structure, rifted formation, and Gondwana subduction history, *Geochim. Geophys. Geosyst.*, 9, Q07004, doi:10.1029/2007GC001855.
- Donelick, R. A. (1993), Method of fission track analysis utilizing bulk chemical etching of apatite, Google Patents.
- Donelick, R. A., P. B. O'Sullivan, and R. A. Ketcham (2005), Apatite fission-track analysis, *Rev. Mineral. Geochem.*, 58(1), 49–94.
- Dunkl, I. (2002), Trackkey: A Windows program for calculation and graphical presentation of fission track data, *Comput. Geosci.*, 28(1), 3–12.
- Eagles, G., K. Gohl, and R. D. Larter (2004), High resolution animated tectonic reconstruction of the South Pacific and West Antarctic margin, *Geochim. Geophys. Geosyst.*, 5, Q07002, doi:10.1029/2003GC000657.
- Eggs, S. M., J. D. Woodhead, L. P. J. Kinsley, G. E. Mortimer, P. Sylvester, M. T. McCulloch, J. M. Hergt, and M. R. Handler (1997), A simple method for the precise determination of ≥ 40 trace elements in geological samples by ICPMS using enriched isotope internal standardisation, *Chem. Geol.*, 134(4), 311–326.
- Farley, K. A. (2002), (U-Th)/He dating: Techniques, calibrations, and applications, *Rev. Mineral. Geochem.*, 47(1), 819–844.
- Farley, K. A., R. A. Wolf, and L. T. Silver (1996), The effects of long alpha-stopping distances on (U-Th)/He ages, *Geochim. Cosmochim. Acta*, 60(21), 4223–4229.
- Favier, L., G. Durand, S. L. Cornford, G. H. Gudmundsson, O. Gagliardini, F. Gillet-Chaulet, T. Zwinger, A. J. Payne, and A. M. Le Brocq (2014), Retreat of Pine Island Glacier controlled by marine ice-sheet instability, *Nat. Clim. Change*, 2094, 1–5.
- Flowers, R. M., R. A. Ketcham, D. L. Shuster, and K. A. Farley (2009), Apatite (U-Th)/He thermochronometry using a radiation damage accumulation and annealing model, *Geochim. Cosmochim. Acta*, 73(8), 2347–2365.
- Fretwell, P., et al. (2013), Bedmap2: Improved ice bed, surface and thickness datasets for Antarctica, *Cryosphere*, 7(1), 375–393.
- Galbraith, R. F. (1981), On statistical models for fission track counts, *J. Int. Assoc. Math. Geol.*, 13(6), 471–478.
- Galbraith, R. F., and P. F. Green (1990), Estimating the component ages in a finite mixture, *Nucl. Tracks Radiat. Meas.*, 17, 196–206.
- Gleadow, A. J. W., I. R. Duddy, P. F. Green, and J. F. Lovering (1986), Confined fission track lengths in apatite: A diagnostic tool for thermal history analysis, *Contrib. Mineral. Petrol.*, 94(4), 405–415.
- Gohl, K. (2012), Basemant control on past ice sheet dynamics in the Amundsen Sea Embayment, West Antarctica, *Palaeogeogr. Palaeoclimatol. Palaeoecol.*, 335, 35–41.
- Gohl, K., A. Denk, G. Eagles, and F. Wobbe (2013a), Deciphering tectonic phases of the Amundsen Sea Embayment shelf, West Antarctica, from a magnetic anomaly grid, *Tectonophysics*, 585, 113–123.
- Gohl, K., G. Uenzelmann-Neben, R. D. Larter, C.-D. Hillenbrand, K. Hochmuth, T. Kalberg, E. Weigelt, B. Davy, G. Kuhn, and F. O. Nitsche (2013b), Seismic stratigraphic record of the Amundsen Sea Embayment shelf from pre-glacial to recent times: Evidence for a dynamic West Antarctic ice sheet, *Mar. Geol.*, 344, 115–131.
- Green, P. F. (1981), A criticism of the paper entitled "A practical method of estimating standard error of age in the fission track dating method" by Johnson, McGee and Naeser, *Nucl. Tracks*, 5(3), 317–323.
- Green, P. F. (1985), Comparison of zeta calibration baselines for fission-track dating of apatite, zircon and sphene, *Chem. Geol.*, 58(1–2), 1–22.
- Groh, A., H. Ewert, M. Scheinert, M. Fritsche, A. Rülke, A. Richter, R. Rosenau, and R. Dietrich (2012), An investigation of glacial isostatic adjustment over the Amundsen Sea sector, West Antarctica, *Global Planet. Change*, 98–99, 45–53.
- Grunow, A. M., D. V. Kent, and I. W. D. Dalziel (1991), New paleomagnetic data from Thurston Island: Implications for the tectonics of West Antarctica and Weddell Sea opening, *J. Geophys. Res.*, 96, 17,935–17,954, doi:10.1029/91JB01507.
- Hughes, T. J. (1981), The weak underbelly of the West Antarctic ice-sheet, *J. Glaciol.*, 27(97), 518–525.
- Hurfurd, A. J. (1990), Standardization of fission track dating calibration: Recommendation by the Fission Track Working Group of the I.U.G.S. Subcommittee on Geochronology, *Chem. Geol.*, 80(2), 171–178.

- Hurford, A. J., and P. F. Green (1982), A users' guide to fission track dating calibration, *Earth Planet. Sci. Lett.*, *59*(2), 343–354.
- Hurford, A. J., and P. F. Green (1983), The zeta age calibration of fission-track dating, *Chem. Geol.*, *41*, 285–317.
- Jordan, T. A., F. Ferraccioli, D. G. Vaughan, J. W. Holt, H. Corr, D. D. Blankenship, and T. M. Diehl (2010), Aerogravity evidence for major crustal thinning under the Pine Island Glacier region (West Antarctica), *Geol. Soc. Am. Bull.*, *122*, 714–726.
- Joughin, I., and R. B. Alley (2011), Stability of the West Antarctic ice sheet in a warming world, *Nat. Geosci.*, *4*(8), 506–513.
- Joughin, I., B. E. Smith, and D. M. Holland (2010), Sensitivity of 21st century sea level to ocean-induced thinning of Pine Island Glacier, Antarctica, *Geophys. Res. Lett.*, *37*, L20502, doi:10.1029/2010GL044819.
- Kalberg, T., and K. Gohl (2014), The crustal structure and tectonic development of the continental margin of the Amundsen Sea Embayment, West Antarctica: Implications from geophysical data, *Geophys. J. Int.*, *198*(1), 327–341.
- Ketcham, R. A. (2005), Forward and inverse modeling of low-temperature thermochronometry data, *Rev. Mineral. Geochem.*, *58*(1), 275–314.
- Ketcham, R. A., A. Carter, R. A. Donelick, J. Barbarand, and A. J. Hurford (2007a), Improved modeling of fission-track annealing in apatite, *Am. Mineral.*, *92*(5–6), 799–810.
- Ketcham, R. A., A. Carter, R. A. Donelick, J. Barbarand, and A. J. Hurford (2007b), Improved measurement of fission-track annealing in apatite using c-axis projection, *Am. Mineral.*, *92*(5–6), 789–798.
- Ketcham, R. A., C. Gautheron, and L. Tassan-Got (2011), Accounting for long alpha-particle stopping distances in (U–Th–Sm)/He geochronology: Refinement of the baseline case, *Geochim. Cosmochim. Acta*, *75*(24), 7779–7791.
- Kipf, A., N. Mortimer, R. Werner, K. Gohl, P. Van Den Bogaard, F. Hauff, and K. Hoernle (2012), Granitoids and dykes of the Pine Island Bay region, West Antarctica, *Antarct. Sci.*, *24*(05), 473–484.
- Landis, C. A., H. J. Campbell, J. G. Begg, D. C. Mildenhall, A. M. Paterson, and S. A. Trewick (2008), The Waipounamu erosion surface: Questioning the antiquity of the New Zealand land surface and terrestrial fauna and flora, *Geol. Mag.*, *145*(02), 173–197.
- Laslett, G. M., W. S. Kendall, A. J. W. Gleadow, and I. R. Duddy (1982), Bias in measurement of fission-track length distributions, *Nucl. Tracks Radiat. Meas.*, *6*(2–3), 79–85.
- Lawver, L., J. Royer, D. Sandwell, and C. Scotese (1991), Evolution of the Antarctic continental margins, in *Geological Evolution of Antarctica*, edited by M. R. A. Thomson, J. A. Crame, and J. W. Thomson, pp. 533–539, Cambridge Univ. Press, Cambridge, U. K.
- LeMasurier, W. E. (1990), Late Cenozoic volcanism on the Antarctic plate: An overview, in *Volcanoes of the Antarctic Plate and Southern Oceans*, edited by W. E. LeMasurier and J. W. Thomson, pp. 1–17, AGU, Washington, D. C.
- LeMasurier, W. E. (2006), What supports the Marie Byrd Land dome? An evaluation of potential uplift mechanisms in a continental rift system, in *Antarctica: Contributions to Global Earth Sciences*, pp. 299–302, Springer Verlag, Berlin.
- LeMasurier, W. E. (2008), Neogene extension and basin deepening in the West Antarctic rift inferred from comparisons with the East African rift and other analogs, *Geology*, *36*(3), 247–250.
- LeMasurier, W. E., and C. A. Landis (1996), Mantle-plume activity recorded by low-relief erosion surfaces in West Antarctica and New Zealand, *Geol. Soc. Am. Bull.*, *108*(11), 1450–1466.
- Lopatin, B. G., and E. M. Orlenko (1972), Outline of the geology of Marie Byrd Land and the Eights Coast, in *Antarctic Geology and Geophysics*, edited by R. J. Adie, pp. 245–250, Universitetsforlaget, Oslo.
- Lovera, O. M., M. Grove, T. Mark Harrison, and K. I. Mahon (1997), Systematic analysis of K-feldspar 40Ar/39Ar step heating results: I. Significance of activation energy determinations, *Geochim. Cosmochim. Acta*, *61*(15), 3171–3192.
- Mehling, A. (2015), Hornblende-Plagioklas Thermobarometrie an Graniten der Backer Inseln in der Pine Island Bay, Westantarktis, Bachelor thesis, 50 pp., Univ. of Bremen.
- Mercer, J. H. (1978), West Antarctic ice sheet and CO₂ greenhouse effect—Threat of disaster, *Nature*, *271*(5643), 321–325.
- Mouginot, J., E. Rignot, and B. Scheuchl (2014), Sustained increase in ice discharge from the Amundsen Sea Embayment, West Antarctica, from 1973 to 2013, *Geophys. Res. Lett.*, *41*, 1576–1584, doi:10.1002/2013GL059069.
- Mukasa, S. B., and I. W. D. Dalziel (2000), Marie Byrd Land, West Antarctica: Evolution of Gondwana's Pacific margin constrained by zircon U–Pb geochronology and feldspar common-Pb isotopic compositions, *Geol. Soc. Am. Bull.*, *112*(4), 611–627.
- Müller, R. D., K. Gohl, S. C. Cande, A. Goncharov, and A. V. Golynsky (2007), Eocene to Miocene geometry of the West Antarctic Rift System, *Aust. J. Earth Sci.*, *54*(8), 1033–1045.
- Muto, A., S. Anandakrishnan, and R. B. Alley (2013), Subglacial bathymetry and sediment layer distribution beneath the Pine Island Glacier ice shelf, West Antarctica, modeled using aerogravity and autonomous underwater vehicle data, *Ann. Glaciol.*, *54*(64), 27–32.
- Nitsche, F. O., S. S. Jacobs, R. D. Larter, and K. Gohl (2007), Bathymetry of the Amundsen Sea continental shelf: Implications for geology, oceanography, and glaciology, *Geochem. Geophys. Geosyst.*, *8*, Q10009, doi:10.1029/2007GC001694.
- Nitsche, F. O., K. Gohl, R. D. Larter, C. D. Hillenbrand, G. Kuhn, J. A. Smith, S. Jacobs, J. B. Anderson, and M. Jakobsson (2013), Paleo ice flow and subglacial meltwater dynamics in Pine Island Bay, West Antarctica, *Cryosphere*, *7*(1), 249–262.
- Palais, J. M., P. R. Kyle, W. C. McIntosh, and D. Seward (1988), Magmatic and phreatomagmatic volcanic activity at Mt. Takahe, West Antarctica, based on tephra layers in the Byrd ice core and field observations at Mt. Takahe, *J. Volcanol. Geotherm. Res.*, *35*(4), 295–317.
- Pankhurst, R. J., I. L. Millar, A. M. Grunow, and B. C. Storey (1993), The Pre-Cenozoic magmatic history of the Thurston Island Crustal Block, west Antarctica, *J. Geophys. Res.*, *98*, 11,835–11,849, doi:10.1029/93JB01157.
- Pankhurst, R. J., S. D. Weaver, J. D. Bradshaw, B. C. Storey, and T. R. Ireland (1998), Geochronology and geochemistry of pre-Jurassic superterranes in Marie Byrd Land, Antarctica, *J. Geophys. Res.*, *103*, 2529–2547, doi:10.1029/97JB02605.
- Panter, K. S., S. R. Hart, P. Kyle, J. Blusztajn, and T. Wilch (2000), Geochemistry of Late Cenozoic basalts from the Cray Mountains: Characterization of mantle sources in Marie Byrd Land, Antarctica, *Chem. Geol.*, *165*(3–4), 215–241.
- Prenzel, J., F. Lisker, M. Balestrieri, A. Läufer, and C. Spiegel (2013), The Eisenhower Range, Transantarctic Mountains: Evaluation of qualitative interpretation concepts of thermochronological data, *Chem. Geol.*, *352*, 176–187.
- Prenzel, J., F. Lisker, M. Elsner, R. Schöner, M. Balestrieri, A. Läufer, U. Berner, and C. Spiegel (2014), Burial and exhumation of the Eisenhower Range, Transantarctic Mountains, based on thermochronological, sedimentary rock maturity and petrographic constraints, *Tectonophysics*, *630*, 113–130.
- Pritchard, H. D., R. J. Arthern, D. G. Vaughan, and L. A. Edwards (2009), Extensive dynamic thinning on the margins of the Greenland and Antarctic ice sheets, *Nature*, *461*(7266), 971–975.
- Rahn, M., and D. Seward (2000), How many track lengths do we need?, *Newsl. Int. Fission-Track Commun.*, *10*/1(20), 12–15.
- Rey, P., O. Vanderhaeghe, and C. Teyssier (2001), Gravitational collapse of the continental crust: Definition, regimes and modes, *Tectonophysics*, *342*(3–4), 435–449.
- Rignot, E., J. L. Bamber, M. R. Van Den Broeke, C. Davis, Y. H. Li, W. J. Van De Berg, and E. Van Meijgaard (2008), Recent Antarctic ice mass loss from radar interferometry and regional climate modelling, *Nat. Geosci.*, *1*(2), 106–110.

- Rignot, E., J. Mouginot, and B. Scheuchl (2011), Antarctic grounding line mapping from differential satellite radar interferometry, *Geophys. Res. Lett.*, **38**, L10504, doi:10.1029/2011GL047109.
- Rignot, E., S. Jacobs, J. Mouginot, and B. Scheuchl (2013), Ice-shelf melting around Antarctica, *Science*, **341**(6143), 266–270.
- Shuster, D. L., R. M. Flowers, and K. A. Farley (2006), The influence of natural radiation damage on helium diffusion kinetics in apatite, *Earth Planet. Sci. Lett.*, **249**(3), 148–161.
- Siddoway, C. (2008), Tectonics of the West Antarctic Rift System: New light on the history and dynamics of distributed intracontinental extension, in *Antarctica: A Keystone in a Changing World*, pp. 91–114, The National Academies Press, Washington, D. C.
- Smith, J. A., C. D. Hillenbrand, G. Kuhn, R. D. Larter, A. G. C. Graham, W. Ehrmann, S. G. Moreton, and M. Forwick (2011), Deglacial history of the West Antarctic Ice Sheet in the western Amundsen Sea Embayment, *Quat. Sci. Rev.*, **30**(5–6), 488–505.
- Spiegel, C., B. Kohn, A. Raza, T. Rainer, and A. Gleadow (2007), The effect of long-term low-temperature exposure on apatite fission track stability: A natural annealing experiment in the deep ocean, *Geochim. Cosmochim. Acta*, **71**(18), 4512–4537.
- Spiegel, C., B. Kohn, D. Belton, Z. Berner, and A. Gleadow (2009), Apatite (U–Th–Sm)/He thermochronology of rapidly cooled samples: The effect of He implantation, *Earth Planet. Sci. Lett.*, **285**(1–2), 105–114.
- SPRITE-Group, and C. G. Boyer (1992), The southern rim of the Pacific Ocean: Preliminary geologic report of the Amundsen Sea–Bellingshausen Sea cruise of the Polar Sea, *Antarct. J. U. S.*, **27**, 11–14.
- Storti, F., M. L. Balestrieri, F. Balsamo, and F. Rossetti (2008), Structural and thermochronological constraints to the evolution of the West Antarctic Rift System in central Victoria Land, *Tectonics*, **27**, TC4012, doi:10.1029/2006TC002066.
- Tagami, T., and C. Shimada (1996), Natural long-term annealing of the zircon fission track system around a granitic pluton, *J. Geophys. Res.*, **101**, 8245–8255, doi:10.1029/95JB02885.
- Taylor, B. (1969), Proposition VII, theorem 3, corollary 2, in *Methodus Incrementorum Directa et Inversa [Direct and Reverse Methods of Incrementation]* (London, 1715), edited, pp. 329–332, Harvard Univ. Press, Cambridge, Mass.
- Vermeech, P. (2008), Three new ways to calculate average (U–Th)/He ages, *Chem. Geol.*, **249**(3–4), 339–347.
- Wagner, G. A., A. J. W. Gleadow, and P. G. Fitzgerald (1989), The significance of the partial annealing zone in apatite fission-track analysis: Projected track length measurements and uplift chronology of the transantarctic mountains, *Chem. Geol.*, **79**(4), 295–305.
- Warner, R. C., and J. L. Roberts (2013), Pine Island Glacier (Antarctica) velocities from Landsat7 images between 2001 and 2011: FFT-based image correlation for images with data gaps, *J. Glaciol.*, **59**(215), 571–582.
- Weertman, J. (1974), Stability of the junction between an ice sheet and an ice shelf, *J. Glaciol.*, **13**(67), 3–13.
- Welke, B., K. Licht, A. Hennessy, S. Hemming, E. Pierce Davis, and C. Kassab (2016), Applications of detrital geochronology and thermochronology from glacial deposits to the Paleozoic and Mesozoic thermal history of the Ross Embayment, Antarctica, *Geochem. Geophys. Geosyst.*, **17**, 2762–2780, doi:10.1002/2015GC005941.
- Wilson, D. S., S. S. R. Jamieson, P. J. Barrett, G. Leitchkov, K. Gohl, and R. D. Larter (2012), Antarctic topography at the Eocene–Oligocene boundary, *Palaeogeogr. Palaeoclimatol. Palaeoecol.*, **335–336**, 24–34.
- Wilson, D. S., D. Pollard, R. M. DeConto, S. S. R. Jamieson, and B. P. Luyendyk (2013), Initiation of the West Antarctic Ice Sheet and estimates of total Antarctic ice volume in the earliest Oligocene, *Geophys. Res. Lett.*, **40**, 4305–4309, doi:10.1002/grl.50797.
- Winberry, J. P., and S. Anandakrishnan (2004), Crustal structure of the West Antarctic rift system and Marie Byrd Land hotspot, *Geology*, **32**(11), 977–980.
- Wobbe, F., K. Gohl, A. Chambord, and R. Sutherland (2012), Structure and breakup history of the rifted margin of West Antarctica in relation to Cretaceous separation from Zealandia and Bellingshausen plate motion, *Geochem. Geophys. Geosyst.*, **13**, Q04W12, doi:10.1029/2011GC003742.
- Wobbe, F., A. Lindeque, and K. Gohl (2014), Anomalous South Pacific lithosphere dynamics derived from new total sediment thickness estimates off the West Antarctic margin, *Global Planet. Change*, **123**(Part A), 139–149.
- Wolf, R. A., K. A. Farley, and D. M. Kass (1998), Modeling of the temperature sensitivity of the Apatite (U–Th)/He thermochronometer, *Chem. Geol.*, **148**, 105–114.
- Zachos, J., M. Pagani, L. Sloan, E. Thomas, and K. Billups (2001), Trends, rhythms, and aberrations in global climate 65 Ma to present, *Science*, **292**(5517), 686–693.